Graduate School Form 30
Updated 1/15/2015

PURDUE UNIVERSITY
GRADUATE SCHOOL
Thesis/Dissertation Acceptance

This is to certify that the thesis/dissertation prepared

By Ricardo Emilio Basora Rovira

Entitled
VEHICLE CLASSIFICATION METHOD FOR USE WITH RAPIDLY EMPLACED MOBILE BRIDGES: A SENSITIVITY STUDY

For the degree of Master of Science in Civil Engineering

Is approved by the final examining committee:

Shirley J. Dyke
Chair

Robert J. Connor

Jakob C. Bruhl

To the best of my knowledge and as understood by the student in the Thesis/Dissertation Agreement, Publication Delay, and Certification Disclaimer (Graduate School Form 32), this thesis/dissertation adheres to the provisions of Purdue University's "Policy of Integrity in Research" and the use of copyright material.

Approved by Major Professor(s): Shirley J. Dyke

Approved by: Dulcy M. Abraham 12/1/2015
Head of the Departmental Graduate Program Date

VEHICLE CLASSIFICATION METHOD FOR USE WITH RAPIDLY EMPLACED MOBILE BRIDGES: A SENSITIVITY STUDY

A Thesis

Submitted to the Faculty

of

Purdue University

by

Ricardo E. Basora Rovira

In Partial Fulfillment of the

Requirements for the Degree

of

Master of Science in Civil Engineering

December 2015

Purdue University

West Lafayette, Indiana

To my hero, Selma Basora Rovira. Your sacrifices allowed me to strive for success.

To my parents, sisters, brothers, nieces, nephews and better half.

ACKNOWLEDGMENTS

I would like to thank and recognize Dr. Shirley J. Dyke, my advisor and mentor throughout my graduate studies. Your invaluable guidance has pushed me to find new limits. I also would like to thank the members of my committee, Dr. Robert J. Connor and Lieutenant Colonel Jakob Bruhl, for evaluating my work and providing insightful guidance. A special thanks to Chul Min Yeum and Christian E. Silva Salazar for providing the basis for the feature detection algorithm and finite element model. Your invaluable guidance helped me excel.

A special thanks to the Purdue Military Research Institute, for supporting and funding us military officers and veterans in the road of academic enlightening. Your dedication to our nation's service members is admirable. Also, a special thanks to the Air Force Institute of Technology, Civilian Institution Program, for enabling me to accomplish my dream of being a structural engineer, and believing in the power of education by continuing to develop the Air Force civil engineers.

Thanks to Luna-ARMY SBIR funding, especially Jeff Demo, for continuing to develop our nation's defenses with the latest research. Also, thanks to the members of the Intelligent Infrastructure Systems Laboratory, for providing insightful comments and suggestions to improve my research and search for answers.

The views expressed in this thesis are those of the author and do not reflect the official policy or position of the United States Air Force, Department of Defense, or the U.S. Government.

TABLE OF CONTENTS

Page

Page

LIST OF TABLES

LIST OF FIGURES

Figure Page

SYMBOLS

0_{NxN}	Zeros matrix
A	Transformation matrix
cm	Centimeter
C_{final}	Final damping matrix
E	Modulus of elasticity
$f(x)$	Weak classifier
$F(x)$	Strong classifier
ke	Element stiffness matrix
k_{global}	Global stiffness matrix
K_{global}	Global stiffness matrix, boundary conditions removed
k_{ij}	Stiffness influence coefficient
K_{final}	Final condensed stiffness matrix
kN	Kilonewton
I	Moment of inertia
I_{NxN}	Identity matrix
L_e	Element length
L	Bridge length
m	Meter
m	Mass
m_e	Element mass matrix
m_{global}	Global mass matrix
M_{global}	Global mass matrix, boundary conditions removed
m_{ij}	Mass influence coefficient
M_{final}	Final condensed mass matrix

M_n	n_{th} term in diagonalized modal mass matrix
n	Number of rounds
P	Load
r	Noise ratio
s	Seconds
u	Displacement
$\dot{u}$	Velocity
$\ddot{u}$	Acceleration
U	Input vector
$w(t_i)$	Noise signal
$W(t)$	Uniformly distributed random values
α	Weight of weak classifier
β	Root Mean Square value
μ	Scaling factor
ω_n	n_{th} mode frequency
ϕ_n	n_{th} modeshape
ψ	Deflected shape
σ	Standard deviation
ζ_n	Damping ratio

ABBREVIATIONS

AASHTO	American Association of State Highway and Transportation Officials
AVLB	Armored vehicle launched bridge
CBT	Common bridge transporter
DOF	Degrees of freedom
FFT	Fast Fourier transform
FHWA	Federal Highway Administration
GVW	Gross Vehicle Weight
HMMWV	High Mobility Multipurpose Wheeled Vehicle
Hz	Hertz
km/hr	Kilometers per hour
LRFD	Load and Resistance Factor Design
LTA	Long term average
MLC	Military Load Class
MRAP	Mine Resistant Armored Protected
NIB	National Bridge Inventory
OvO	One versus one
OvR	One versus rest
REB	Rapidly Emplaced Bridge
RMS	Root mean square
SBC	Soil bearing capacity
SBIR	Small Business Research Initiative
STA	Short term average
RSLI	Remaining Service Life Indicators

UC	Unclassified
WIM	Weigh-in-motion

ABSTRACT

Basora Rovira, Ricardo E. MSCE, Purdue University, December 2015. Vehicle Classification Method For Use With Rapidly Emplaced Mobile Bridges: A Sensitivity Study. Major Professor: Shirley J. Dyke.

A feature detection algorithm is developed to determine which type of vehicle crosses a mobile bridge using acceleration responses. The purpose of this thesis is to examine the results sensitivity of the algorithm to various parameters that influence the ability to correctly classify vehicles. Each of these results will play a role in developing the most suitable procedure.

Using numerical and experimental results, the parameters studied are: bridge length, vehicle speed, noise, sensor filtering, and soil conditions. Each parameter is varied individually to determine how much it affects the ability of the method to classify vehicles traversing the bridge. Consideration is given to how parameters could be controlled under real world conditions to yield reliable results. The investigations demonstrate that results vary slightly to noise levels, the length of the bridge is constant once emplaced, sensor filtering setting can be fixed, soil condition impacts are minimum, and the vehicle speed can be controlled if a ground guide is used.

Based on the observations, a generalized procedure is prepared which consists of: creating a database with multiples parameters, controlling the parameters within realistic constraints, and grouping similar vehicle responses. The procedure aims to provide the best environment to produce reliable detection rates.

1. INTRODUCTION

Every bridge designed is determined to have a finite or infinite life. Bridge lifetime is calculated based on the stress ranges produced by vehicle crossings and fatigue performance of the critical components [1]. This estimate assumes that traffic patterns remain constant during the entire life, which is not realistic. However, updated histograms and stress range studies are conducted to determine if a bridge's lifetime has been reduced or can be extended. This issue gets magnified in short span temporary bridges due to variable boundary conditions.

Temporary bridges are used in a myriad of areas such as: military warfare, disaster response, alternate routes, detours, among others. The same bridge may be emplaced at different locations with multiple uses throughout its existence. A very popular form of temporary bridge is the Acrow bridge [2]. Acrow bridges provide relief while permanent bridges are built or repaired. The Federal Highway Administration (FHWA) National Bridge Inventory (NIB) provides guidelines to determine if a bridge is temporary [3]. However, the number of passes and stresses experienced may vary greatly if they are emplaced along a highway as opposed to a rural road. These very different parameters can make the bridge experience either very high stress ranges, establishing a finite life, or very low stress ranges, establishing an infinite life. Various methods and algorithms, both passive and active, have been designed and used to monitor he behavior of our current infrastructure.

Active methods such as weigh-in-motion (WIM) and strain gages are popular in bridges to monitor and update the vehicle histogram. WIM often uses piezoelectric or quartz sensors in order to determine the axle weight, number of axles, speed and gross vehicle weight [4]. However, in order to determine how a bridge behaves when a vehicle crosses, strain gages are installed in specific locations to calculate stresses.

These results help determine if the bridge lifetime changed for the better or worse. However, they do have their limitations.

WIM requires bridge or road modifications to ensure a flushed transition. They are very popular on roads, as they prevent overweight vehicles from damaging our roads and also keep the static scales use to a minimum. However, WIM does not replace static scales due to a restriction on the error tolerance [5]. Adaptive and error reducing algorithms have been developed to increase their accuracy and continue to identify the amount of overweight vehicles in our roads [4] [5]. Despite advances to improve the accuracy of the WIM, it does not provide details on how bridges behave, as strain gages do.

Strain gages are used extensively in specific regions of bridges to determine the actual stress ranges experienced. However, strain gages have practical limitations and need to be located in specific regions of the bridge to get the actual critical stress ranges produced by vehicles [6]. Randomly locating strain gages in a bridge would not provide the necessary information to determine bridge serviceability. Installing the strain gages can be a difficult task, especially if access to the critical members that need to be measured is limited. A final passive method, known as fatigue fuses, are also used.

Fatigue fuses are metal legs that are designed to break off after a specific amount of full-load cycles are experienced in a steel bridge [7] [8]. Typically, they are set up with four legs, each one breaking at different full-load cycles. These are both easily and quickly implemented. They can help users know when a stress or bridge lifetime analysis is required, saving time and money. However, various conditions such as overweight vehicles or handling accidents, may cause premature breakdown. This leads to the motivation behind the use of accelerometers for mobile bridge applications.

1.1 Motivation

The Rapidly Emplaced Bridge (REB) System, shown in figure 1.1, is a temporary mobile bridge that can be emplaced in less than 10 minutes in a variety of conditions, for both disaster relief and military operations. Made from low weight aluminum, it can be transported by a Common Bridge Transporter (CBT) or helicopter, can span up to 13 meters in length, and handle vehicle weights up to 100,000 pounds or 45,359 kilograms [7].

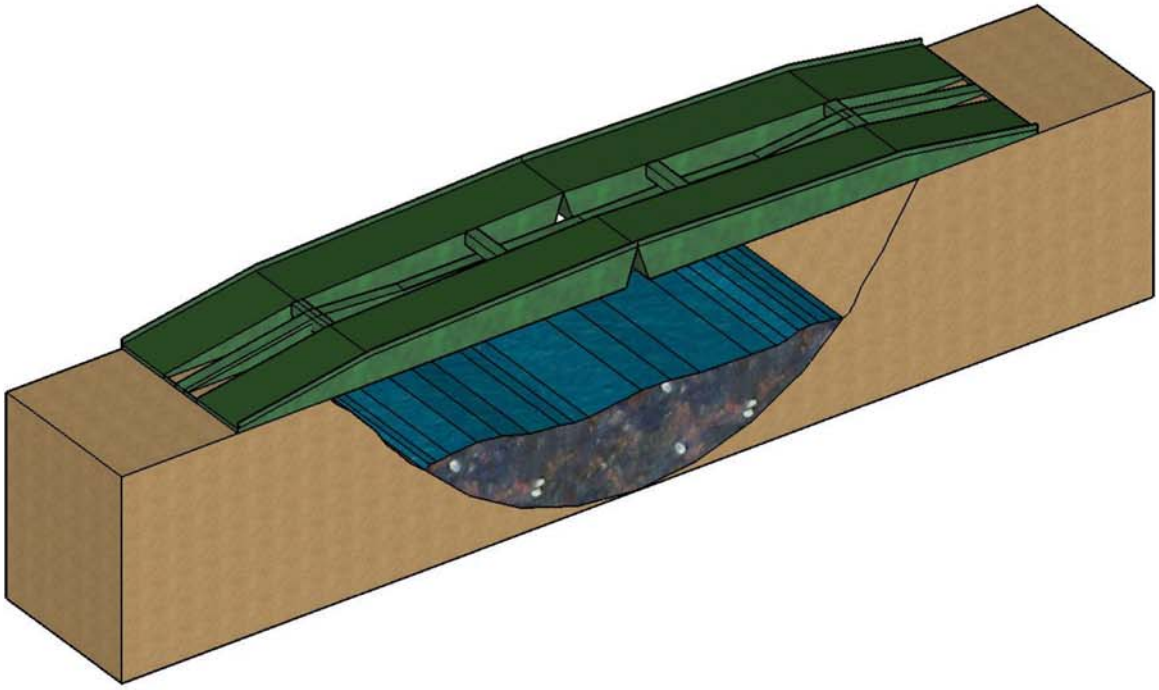

Fig. 1.1. Rapidly Emplaced Bridge

To determine bridge serviceability the REB uses fatigue fuses, a passive indicator. These fuses are known as Remaining Service Life Indicators (RSLI), shown in Figure 1.2. The RSLI provide the only method to determine the condition of the bridge. These fatigue fuses have proven to be effective under most conditions, but some have prematurely failed due to handling or other undetermined reasons.

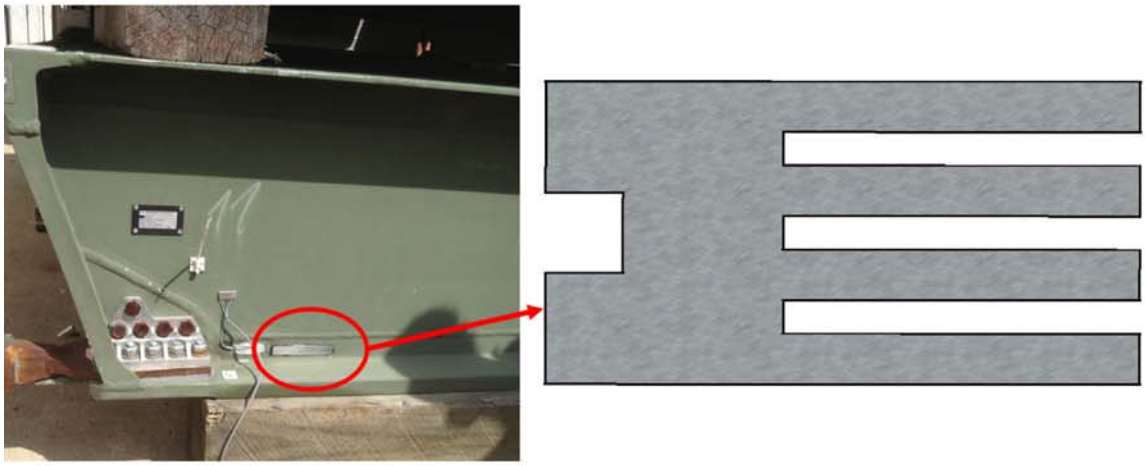

Fig. 1.2. Remaining Service Life Indicator Fatigue Fuses (Courtesy of Jeff Demo)

The REB is normally exposed to a variety of operating conditions. According to [7], the following conditions must be followed for emplacement, shown in Table 1.1

Table 1.1.
REB emplacement and use requirements (from [7])

Parameter	**Limitation**
Soil Bearing Capacity	A minimum of 450 kN/m^2
Load capacity	Maximum Military Load Class (MLC) 50
Span length	Maximum of 13 meters
Bank height differential	Maximum of 1.3 meter
Maximum Speed	40 km/hr for MLC 40 and below, 16 km/hr for MLC 50

Real world emplacements prove to be unforgiving and austere. A new technology to enable usage measurements that does not modify the bridge, is easily installed, can be accessed wirelessly, and consumes low power is needed. Hence the use of low-voltage, low-frequency accelerometers is requested by the user, Luna Innovations, and

funded by the Small Business Research Initiative (SBIR) to actively monitor vehicle passes.

Accelerometers have been used extensively in many applications in civil engineering such as earthquake research [9] and real-time hybrid simulation [10]. They are expected to sustain rough weather and handling, last longer, and maintain the required accuracy, as compared to strain gages. It has been found that strain gages may not perform well in long term harsh settings [11]. Accelerometers can provide the active monitoring the REB needs.

The approach is based on the premise is that each vehicle crossing produces a distinguishable acceleration response. Simulations and experiments are conducted to test and validate this premise. A feature detection algorithm, based on the image processing procedures of Viola-Jones [12] [13], is applied to acceleration spectrograms to classify vehicles crossing a bridge. Spectrograms are used to obtain visual representations of accelerations. Once sufficient spectrograms are generated to create a training database, new vehicles can cross mobile bridges and be classified. However, to acquire a reliable detection rate, a sensitivity study is conducted to examine the influence of certain parameters.

1.2 Problem Statement

The REB needs an active monitoring solution to classify vehicles and maintain a reliable histogram representing usage. Determining what type of vehicles have crossed can help calculate the number of vehicle passes remaining before a repair or retrofit is required. Therefore, the influence of various parameters are studied in numerical and experimental tests to understand how to best implement the method to yield the required accuracies. These tests and recommendations are intended for mobile bridges with a broad range of parameters and not intended for permanent bridges.

The parameters studied in the numerical investigation, section 4, are: bridge length, vehicle speed, noise and sensor filtering. Soil conditions are tested experimen-

tally in section 5. The purpose of this thesis is to study the sensitivity of the vehicle detection algorithm to the aforementioned parameters and develop an implementation recommendation for the REB to garner reliable detection rates.

2. LITERATURE REVIEW

Engineers always strive to understand the behavior of structures to the best of their ability. In the field, they use sensors to study structure behaviors or measure specific data, like the weight of a vehicle using WIM. The Viola-Jones object detection framework, which was developed for objects and images, can be adapted to acceleration spectrograms. This provides new opportunities for use with sensors to study structural behavior. When it is not practical to conduct real world experiments, finite element models are used to represent the behavior of a structure. All these concepts are reviewed in this chapter to understand past successes and what needs to be improved or created.

2.1 Weigh-in-Motion

In transportation, the need to estimate truck weight and monitor road and bridge use has been heavily studied. The different state departments of transportation throughout the United States use and recommend various measuring tools such as: WIM, strain gages, static scales, radio communication, among others [14]. These tools provide quantitative information on vehicle traffic that greatly improves bridge lifetime estimate and reduces uncertainty [15].

WIM systems have been extensively used by federal and state highway agencies. Best practices and handbooks have been published by various authors [16] [17]. Some of their main purposes are to relieve static scale traffic, reduce truck and users transportation times, and most importantly, to protect the transportation infrastructure by detecting and removing overweight vehicles from roadways. Many companies offer commercially available WIM systems that are either permanent or temporary for roads and bridges [18] [19].

A WIM is generally composed of piezoelectric sensors, bending plates, inductive loops, analysis computers and a communications system. Figure 2.1 shows a WIM setup and Figure 2.2 shows a bending plate representation. In such a typical WIM system, an algorithm is developed to determine vehicle speed, axle load, gross vehicle weight and other necessary information for the user. The general algorithm steps to determine the aforementioned information are shown in Table 2.1. The steps outlined are not absolute and vary for different WIM setups, depending on the department.

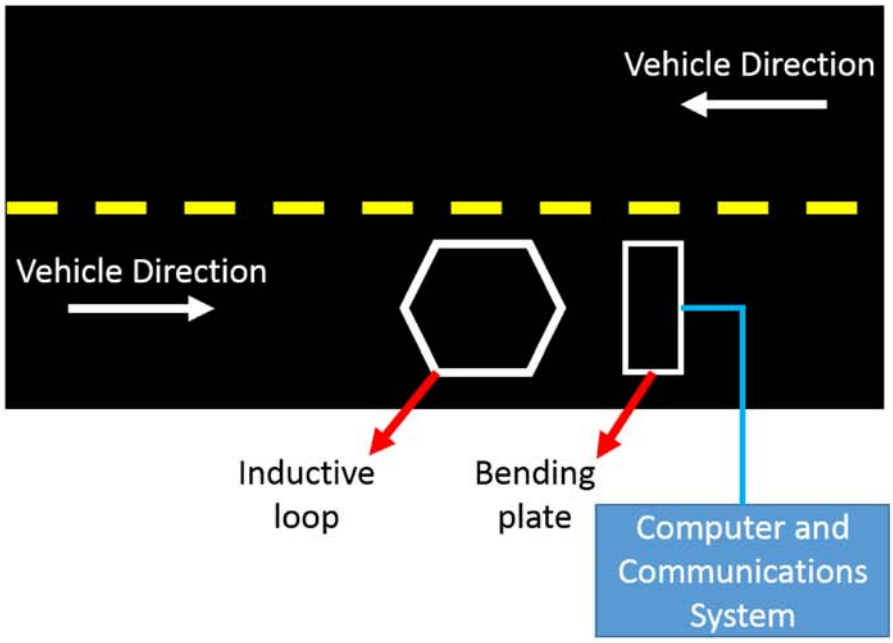

Fig. 2.1. WIM system setup

The algorithm typically uses strain gages and quartz sensors to measure the change in electrical charges produced when a vehicle crosses the bending plate. A vehicle with known axle load, gross vehicle weight (GVW) and speed is used to calibrate the WIM station. Once a new vehicle traverses the bending plate, the electrical charge change is then correlated to loads and speed. The correlation is more accurate when additional parameters are considered to determine vehicle weight, as the relationship is non-linear. Despite a fairly good system, the results are sensitive to speed variation and do not provide enough accuracy to entirely replace static scales [5].

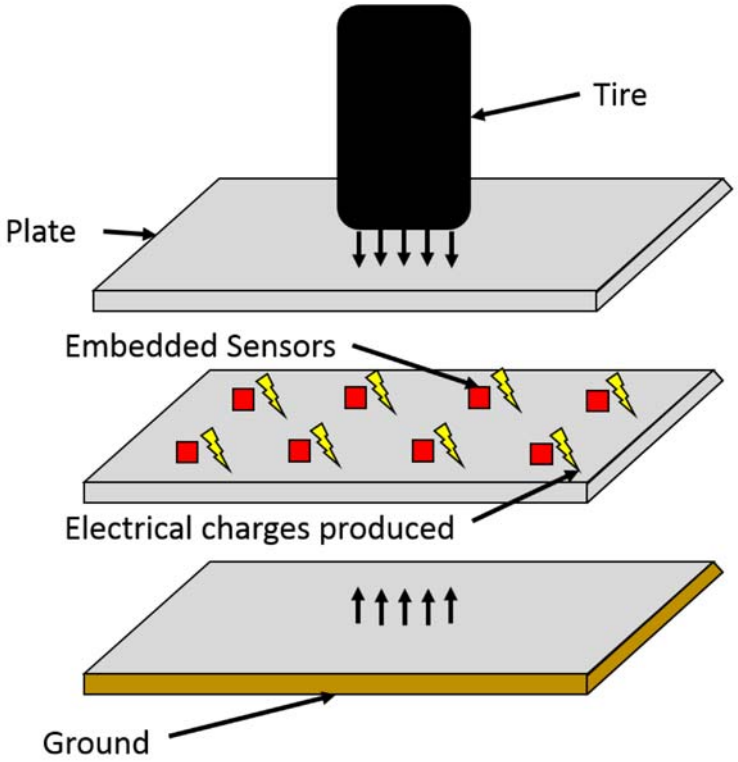

Fig. 2.2. Bending plate representation

Table 2.1.
Generalized WIM algorithm)

Step	Description
1	Inductive loop detects vehicle and starts recording time
2	Bending plate sensors are activated
3	Tires cross the bending plate and produces electrical responses
4	Inductive loop detects vehicle exit
5	Speed is calculated based on the time the inductive loop was activated
6	Electrical responses are converted to axle loads and gross vehicle weight
7	Communication system notifies driver if they need to deviate to static scales

WIM systems have been found to have errors as high as 20%, and ground static scale systems allow 0.1% error rate for certifiable weighting [4] [5]. For these reasons, step 7 in Table 2.1 has yet to be replaced, and static scales are still the most precise and necessary component in weight enforcement. To increase the WIM's effectiveness, additional sensors and a more robust algorithm is required, which requires additional computational power.

Various studies have been conducted for both high speed and slow speed WIM systems to improve the algorithm's reliability and reduce errors in the results. Most WIM overweight detection algorithms are based on a fixed threshold methodology, where a vehicle gets flagged if its GVW exceeds the threshold. However, if GVW follows a normally distributed probability, then slightly overweight vehicles have a 50% chance of passing undetected [5]. As a result, if the threshold is set to 60 kips, then a 61 kips GVW can pass undetected half of the time.

An adaptive threshold algorithm has been developed to increase overweight vehicle capture and reduce static scale closures [5]. Static scales in roads suspend operations if the number of vehicles in line to get weigh is too large and prevents access. In this method, the threshold to detect overweight vehicles is increased as the static scale line grows, preventing closure. For example, if a static scale has a capacity of 20 trucks in line, the WIM initial threshold of 60 kips can be increased to 70 kips when there are 10 trucks in line. Thus, the increase in the threshold reduces misclassification of legal trucks and increases the likelihood of capturing overweight vehicles. However, this algorithm does not replace the static scale, although it does reduce vehicle travel delay somewhat.

Another study was conducted to increase the accuracy of WIM scales above static scale provisions. This methodology could help improve vehicle flow and replace static scales altogether. The study determined that higher mode oscillations produced when vehicles crossed the bending plate were not relevant for weight calculations because they decrease the accuracy [4]. Thus, a method was proposed to reduce non-relevant vehicle oscillations to provide certifiable weight results [4]. However, it only works at

slow speeds below 8 kilometers per hour (km/hr) and needs some additional computational power. Despite improving the movement along the static scales, the speed is too slow and still requires vehicles to deviate from the main road to get approved weight measurements.

The WIM scales have proven to be effective under a specific range of operations. However, its decreased accuracy, heavy computational needs, lack of certifiable weighing, and need to physically change the bridge makes it impractical for mobile bridge applications.

2.2 Finite Element Models

Mobile bridges are emplaced in a variety of locations with different boundary conditions. Physical testing of all parameters is cost prohibitive and impractical. However, the bridge can be idealized as a simply supported beam and analyzed using the finite element method. This provides an excellent alternative to represent the behavior of members or structures at a fraction of the cost of the real world experiments. Various methodologies outlined by Chopra [20] and Craig [21] explain how to apply the finite element method.

Silva considered an assortment of beam finite element models under different boundary conditions [22]. He developed a method to update the model to better represent the vibrating behavior of a bridge. The method consists of comparing the model's mode shapes and frequencies to those of the real structure. The model parameters are changed until the mode shapes and frequencies of the real structure are replicated. The final updated model is then dynamically similar to that of the real structure. Thus, various load cases and scenarios can be investigated to understand the member's behavior without performing real world experiments.

2.3 Feature Detection Method

Human beings are able to differentiate other people's faces thanks to various distinct characteristics each person possesses. These distinguishable features may be the shape of their head, eyes, mouth, nose, ears, among others. As the reader might have experienced, certain people are easier to remember than others due to their distinct features such as moles, hair, skin complexion, birth marks, and scars. The more prominent features a person possesses, the easier it will be for people to remember them. This general concept is actively studied and implemented in the field of computer vision.

2.3.1 Computer Vision

Computer vision presents different methods to acquire, process and analyze images numerically [23] [24]. The applications are endless and can be implemented to any visual representation, in two or three dimensions. A wide variety of applications include: navigation, object detection and retrieval, and measuring distances [23] [24]. Computer vision tends to use the pixels in an image, which are homogeneously shaded squares [23], to compose the numerical values that can be obtained.

Various researchers have used these principles to create and improve algorithms that can detect and remember images. They use it to either find a person in a group or classify them as required. In this thesis, the Viola-Jones object detection framework [12] and rapid identification of images [13] are of special interest.

2.3.2 Viola-Jones Object Detection

Introduced in 2001 [12] and revised in 2004 [13], Viola and Jones presented a quick feature-based object detection system that was 15 times faster than any previous work and yielded very high detection rates. Its success was only limited to aspects such as: lighting, angle, scale, and pose. Even though one might think that with better

resolution comes better results, that is not always true, especially for this framework. Viola-Jones were able to obtain high frame rates with information presented in a gray scale image [12], with detection rates as high as 93%. These high detection rates were obtained as a result of implementing key concepts such as integral image and the boosting learning algorithm.

The integral image computation is the key aspect behind the quickness and effectiveness of the method, as it will be explained in section 3.2.2. When an image is loaded to the algorithm, it is converted to gray scale and its shaded pixels are computed to obtain values for the areas and corners. These values are then extracted using Haar-like features, which aid in determining the strong features. The quick extraction and computation of strong features is possible because of the work done beforehand. Without the integral image, pixel values would have to be calculated for each Haar-like feature after extraction, increasing computational requirements.

Haar-like features are simple rectangular features as compared to steerable filters [13]. Steerable filters adaptively changes filter orientation to determine a specific output such as texture or edges, based on pixels [25]. Pixel based systems can perform detailed analysis of complex images thus, requiring more computational power [13]. However, Haar-like features can provide good image representation that operates much faster than a pixel based system [12]. Additionally, they provided enough resolution to accurately detect individuals in the study, at a fraction of the speed. Thus, if Haar-like features are suitable for face detection, they can be used in simpler images such as spectrograms.

Boosting is a learning algorithm that produces strong classifiers from various weak classifiers, as it will be explained in section 3.2.2. A strong classifier is composed of the sum of weak classifiers, and a weak classifier is composed of strong features found in an image, extracted by the Haar-like features. Viola and Jones used the AdaBoost learning algorithm, due to its simple efficiency of creating classifiers [13]. Their work aggressively removes unnecessary weak features and highlights strong critical features for detection, based on the Freund and Schapire methodology [26]. The algorithm

focuses on using as much distinct weak features as required by the user to create the strong classifier. These iteration produces robust strong classifiers to classify images.

The Viola-Jones object detection framework has inspired multiple innovations and research in the computer vision field. The quickness and effectiveness without much computational requirements appeals to researchers. An implementation study in bridge structures is being conducted to detect damage using images [27].

Yeum is using the Viola-Jones methodology to detect cracks near bolts using pictures from different angles, processed through various methods [27]. Utilizing Haar-like features, images of bolts with and without cracking, from various angles and lighting conditions, were used to create the training classifiers through the gentle boost learning algorithm. When tested from various angles and filters, crack conditions were detected 98% of the time. The successful implementation generates the possibility for automated visual bridge inspections using only images [27].

Visual inspection of bridges is limited by accessibility, environment, and the size of the damage. Using Viola-Jones methodology removes the subjective human effect and provides reliable results and access to areas that were impossible to reach before. The successful implementation of the Viola-Jones methodology shows promising applications in other vision based detection or classification problems.

3. BACKGROUND AND METHODOLOGY

This chapter summarizes the creation and use of the finite element model and the feature detection algorithm.

3.1 Finite Element Model

Finite element models are intended to model real world behavior. Computer programs such as MATLAB, Abaqus, and SAP 2000 can be used to develop such model. The finite element model for this study is developed in MATLAB [28] and follows the procedure outlined by Silva [22]. It simulates the special case of a vehicle crossing a bridge and provides acceleration response at different locations.

3.1.1 Assumptions, parameters, and Limitations

The finite element model provides a representation of the bridge response when vehicles cross. It is created here to provide a testbed to evaluate the feature detection algorithm performance, which parameter variations affect performance the most, and how to improve the results. As with every numerical model, assumptions are needed to conduct simulations, shown in Table 3.1.

Although the REB is a non-homogeneous bridge, a homogeneous beam model is used here to generate a representative set of behaviors and results. The simulation is used to model a vehicle crossing a general mobile bridge and not to recreate the REB response. Similar dynamic properties are used in the beam model to represent the REB.

The following beam properties are inputs to the simulations: cross sectional area, modulus of elasticity, moment of inertia, specific weight, and bridge length. Ad-

Table 3.1.
Finite element model assumptions

Number	Assumption
1	Bridge is modeled as a homogeneous simply supported beam
2	Soil conditions cannot be varied
3	Bridge length can be varied
4	Vehicle axle loads are represented as moving point loads
5	Each node provides acceleration responses
6	Vehicle speed is constant while crossing the beam

ditional simulation parameters can be varied such as: vehicle load and speed, and acceleration response noise. The numerical algorithm created follows the steps shown in Table 3.2.

Table 3.2.
Finite element model steps

Step	Description
1	Bridge properties, number of elements, and parameters are selected
2	Mass and stiffness matrix computed
3	Apply static condensation
4	Modal damping computed
5	State-space system model created
6	Input vehicle load with desired speed
7	Linear simulations computed
8	Acceleration responses are obtained

In this study, our interest lies in focusing on the vertical acceleration. Each acceleration response result is obtained using outputs co-located with the nodes of the

elements. The node location depends on the number of elements, which can be modified as needed. Typically, the number of elements is based on the computational time and capabilities that are available, as well as the smoothness of the response required.

Figure 3.1 shows the convergence of maximum acceleration responses captured at mid-span when an MLC 40 crosses a 13 meter bridge. When 10 elements or less are used, the differences are too large and do not provide reliable results. Therefore, 10 elements or less are not an option for our simulations. Additionally, it is evident that from 12 elements forward, the maximum values remain fairly similar. Other vehicle classes and lengths also demonstrate similar convergence patterns. Thus, this numerical study uses 12 elements, which provide enough reliable data to conduct simulations.

Number of elements	Mid-span max acceleration (m/S²)
20	1.47
18	1.51
16	1.32
12	1.56
10	43.19
8	141.41
6	190.43

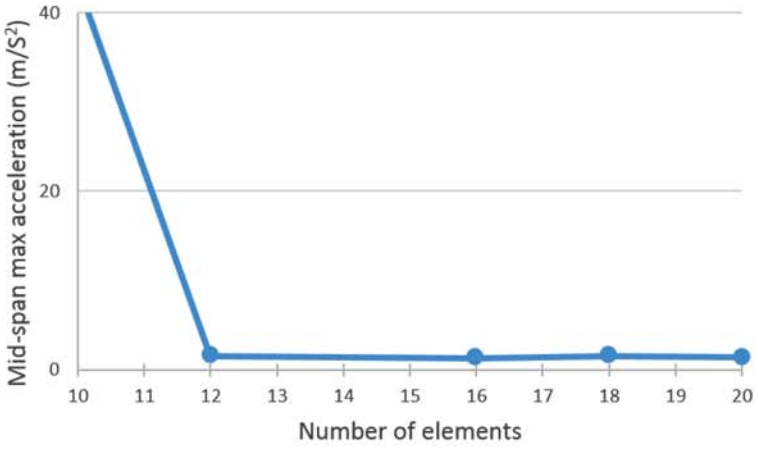

Fig. 3.1. Convergence of acceleration responses as the number of elements increases

The equation of motion (3.1) is the starting point to analyze the problem.

$$M\ddot{u} + C\dot{u} + ku = P(t) \tag{3.1}$$

This second order differential equation is analyzed using the finite element approach. To do so, the mass, stiffness and damping matrices are computed, as shown in the next section.

3.1.2 Mass, Stiffness and Damping Matrix

To calculate the mass and stiffness matrices, the degrees of freedom (DOF) at each node have been idealized as vertical displacement i and rotation j [20] [22]. Using the principal of virtual displacements [20], the stiffness influence coefficient k_{ij} is estimated as

$$k_{ij} = \int_0^{L_e} EI(x)\psi_i''(x)\psi_j''(x)dx \tag{3.2}$$

where L_e is the length of the element or $L/elements$, E is the modulus of elasticity, I is the moment of inertia, and ψ is the assumed deflective shape. ψ_i is selected as $sin(kx\pi/L)$, where L is the length of the bridge and k is the modeshape. The stiffness of each element, k_e can be expressed as [20] [22]

$$[k_e] = \frac{8EI}{L_e^3}\begin{pmatrix} 12 & 3L_e & -12 & 3L_e \\ 3L_e & L_e^2 & -3L_e & L_e^2/2 \\ -12 & -3L_e & -12 & -3L_e \\ 3L_e & L_e^2 & -3L_e & L_e^2/2 \end{pmatrix} \tag{3.3}$$

Similarly, the mass influence coefficient m_{ij} is estimated as

$$m_{ij} = \int_0^{L_e} m(x)\psi_i(x)\psi_j(x)dx \tag{3.4}$$

The mass of each element, m_e is expressed as [20] [22]

$$[m_e] = \frac{mL_e}{420}\begin{pmatrix} 156 & 22L_e & 54 & -13L_e \\ 22L_e & 4L_e^2 & 13L_e & -3L_e^2 \\ 54 & 13L_e & 156 & -22L_e \\ -13L_e & -3L_e^2 & -22L_e & 4L_e^2 \end{pmatrix} \tag{3.5}$$

The element stiffness and mass matrices are calculated using local DOF. They are then converted to the global mass and stiffness matrices, $[m_{global}]$ and $[k_{global}]$, using transformation matrices, $[A]$. Equation 3.6 shows how the conversion occurs to obtain the global matrices.

$$[k_{global}] = \sum_{i=1}^{n} [A_{e_i}^T][k_{e_i}][A_{e_i}] \; and \; [m_{global}] = \sum_{i=1}^{n} [A_{e_i}^T][m_{e_i}][A_{e_i}] \tag{3.6}$$

where A_{e_i} is the i_{th} transformation matrix for the i_{th} element and n is the number of elements. For example, Figure 3.2 shows a beam divided in three elements with eight DOF.

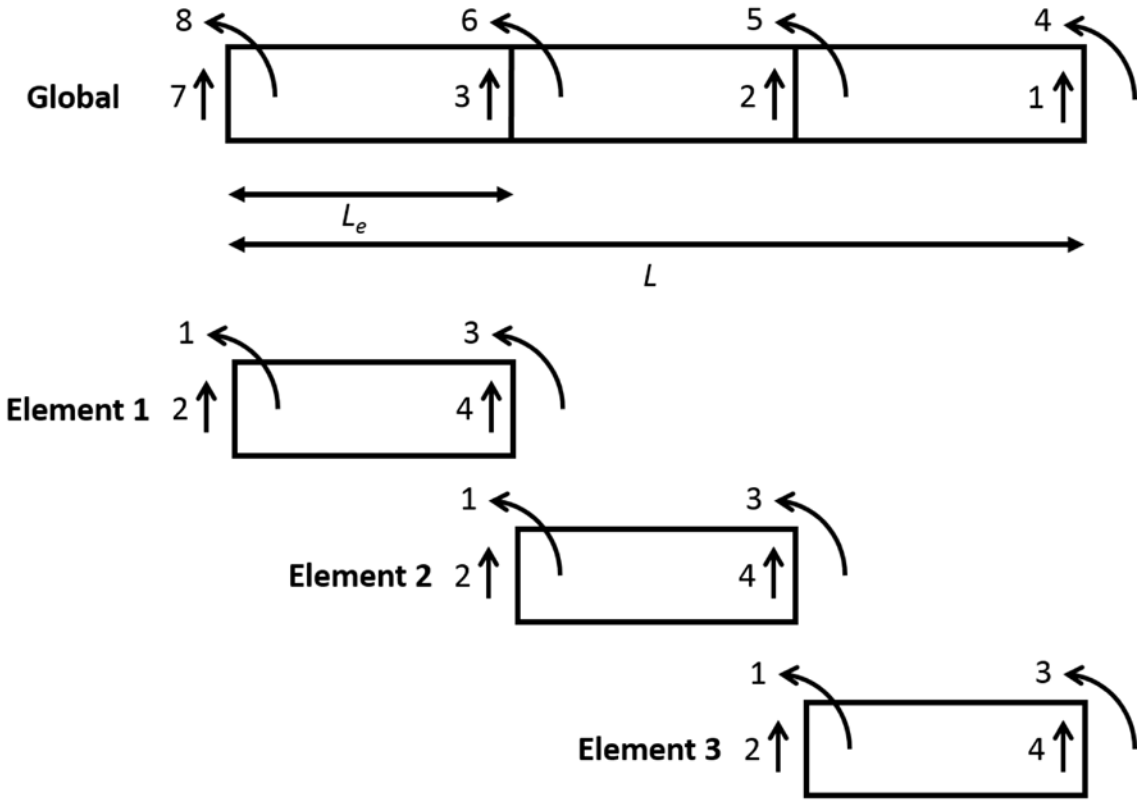

Fig. 3.2. Global and element degrees of freedom

The transpose transformation matrices $[A]$ for the example, are shown in equation 3.7.

$$A^T_{elem1} = \begin{pmatrix} 0 & 0 & 0 & 0 \\ 0 & 0 & 1 & 0 \\ 0 & 0 & 0 & 0 \\ 0 & 0 & 0 & 0 \\ 0 & 0 & 0 & 0 \\ 0 & 0 & 0 & 1 \\ 1 & 0 & 0 & 0 \\ 0 & 1 & 0 & 0 \end{pmatrix} A^T_{elem2} = \begin{pmatrix} 0 & 0 & 1 & 0 \\ 1 & 0 & 0 & 0 \\ 0 & 0 & 0 & 0 \\ 0 & 0 & 0 & 1 \\ 0 & 1 & 0 & 0 \\ 0 & 0 & 0 & 0 \\ 0 & 0 & 0 & 0 \\ 0 & 0 & 0 & 0 \end{pmatrix} A^T_{elem3} = \begin{pmatrix} 0 & 0 & 0 & 0 \\ 0 & 0 & 1 & 0 \\ 0 & 0 & 0 & 0 \\ 0 & 0 & 0 & 0 \\ 0 & 0 & 0 & 0 \\ 0 & 0 & 0 & 1 \\ 1 & 0 & 0 & 0 \\ 0 & 1 & 0 & 0 \end{pmatrix} \tag{3.7}$$

Continuing the example, each $[m_{global}]$ and $[k_{global}]$ analytically obtained is an 8x8 matrix. Since it is assumed that soil conditions do not vary and the beam is simply supported, the boundary conditions are applied. Thus, DOF 1, 4, 7, and 8 are set to zero, leaving the 4x4 $[M_{global}]$ and $[K_{global}]$ matrix with DOF 2, 3, 5, and 6. To further simplify the problem, static condensation is applied.

Static condensation removes the rotational DOF's, assuming they are massless [20]. The 4x4 $[M_{global}]$ and $[K_{global}]$ matrices can be subdivided into multiple 2x2 matrices as follows

$$[M_{global}] = \begin{pmatrix} [m_{aa}] & [m_{a0}] \\ [m_{0a}] & [m_{00}] \end{pmatrix} \; or \; [K_{global}] = \begin{pmatrix} [k_{aa}] & [k_{a0}] \\ [k_{0a}] & [k_{00}] \end{pmatrix} \tag{3.8}$$

Thus, DOF 5 and 6 are removed from consideration by applying the following equation

$$[m_{aa}]\ddot{u} + [k_{aa}]u + [k_{a0}]u_0 = p(t) \tag{3.9}$$

and

$$[k_{0a}]u + [k_{00}]u_0 = 0 \tag{3.10}$$

where u_0 are the DOF without mass.

$$u_0 = -[k_{00}^{-1}][k_{0a}]u \tag{3.11}$$

Substituting, the final condensed stiffness matrix is

$$[M_{final}] = [m_{aa}] - [m_{0a}^T][m_{00}^{-1}][m_{0a}] \tag{3.12}$$

and similarly, the final condensed mass matrix is

$$[K_{final}] = [k_{aa}] - [k_{0a}^T][k_{00}^{-1}][k_{0a}] \tag{3.13}$$

The resulting $[M_{Final}]$ and $[K_{Final}]$ correspond to only vertical DOF's, simplifying the calculations. For Figure 3.2, these results produce a simpler 2x2 mass and stiffness matrix. MATLAB [28] is used to perform matrix operations quicker. For our 12 element model, the final mass and stiffness matrices yields 11x11 matrices. With the $[M_{Final}]$ and $[K_{Final}]$, the damping can be computed.

Various methods can be used to compute the damping matrix such as Rayleigh, Caughey and modal. Under the assumption that a mobile bridge has similar damping throughout [21], modal damping is used because a chosen damping ratio can be enforced for each mode instead of just a few. Following known procedures for calculating modal damping [20] [21], $[C_{Final}]$ is computed as

$$[C_{Final}] = [M_{Final}](\sum_{n=1}^{N} \frac{2\zeta\omega_n}{M_n}\phi_n\phi_n^T)[M_{Final}] \tag{3.14}$$

where ζ_n is the n_{th} mode damping ratio, ω_n is the frequency of the n^{th} modeshape, and M_n is the diagonalized modal mass matrix. In this model, a damping ratio of 2% is applied, assuming a working stress level or a welded steel structure [20]. With the final mass, stiffness, and damping matrices, the equation of motion (3.1) is written as

$$M_{Final}\ddot{u} + C_{Final}\dot{u} + K_{Final}u = P(t) \tag{3.15}$$

Next, this equation is put in state-space form for simulation.

3.1.3 State Space

State-space is a commonly used approach to write higher order equations of motion as multiple first order differential equations [21]. Therefore, equation 3.15 is converted to a first order differential equation by assuming the following [29]:

$$z = \begin{pmatrix} u \\ \dot{u} \end{pmatrix} \; where \; z_1 = u \; and \; z_2 = \dot{u} = \dot{z_1} \tag{3.16}$$

The second order differential equation is rewritten as a first order by substituting z_1 and z_2

$$M_{Final}\dot{z_2} + C_{Final}z_2 + K_{Final}z_1 = P(t) \tag{3.17}$$

and then solving for the differential terms as

$$\ddot{u} = \dot{z_2} = [M_{final}^{-1}]P(t) - [M_{final}^{-1}][C_{final}]z_2 - [M_{final}^{-1}][K_{final}]z_1 \tag{3.18}$$

These equation are then expressed in standard state-space form, with a state and output equation [29].

$$State \; Equation: \; \dot{z} = [A]z + [B]P(t) \tag{3.19}$$

$$Output \; Equation: \; u = [C]z + [D]P(t) \tag{3.20}$$

where,

$$A = \begin{pmatrix} 0_{NxN} & I_{NxN} \\ -M_{Final}^{-1}K_{Final} & -M_{Final}^{-1}C_{Final} \end{pmatrix} and \; B = \begin{pmatrix} 0_{NxN} \\ -M_{Final}^{-1} \end{pmatrix} \tag{3.21}$$

and,

$$C = \begin{pmatrix} I_{NxN} & 0_{MxN} \\ 0_{NxN} & I_{NxN} \\ -M_{Final}^{-1}K_{Final} & -M_{Final}^{-1}C_{Final} \end{pmatrix} and \; D = \begin{pmatrix} 0_{NxN} \\ -M_{Final}^{-1} \end{pmatrix} \tag{3.22}$$

where I_{NxN} is the identity matrix of size NxN and 0_{NxN} is the zeros matrix of size NxN. Once the state and output equations have been assembled, the state-space system is created in MATLAB. To simulate the system, the input vector, U, is then computed as a function of time.

3.1.4 Loading Procedure

The input vector U represents the external force applied to the mobile bridge. Figure 3.3 shows a simplified representation of a vehicle moving across the beam, where the tires are modeled as two point loads.

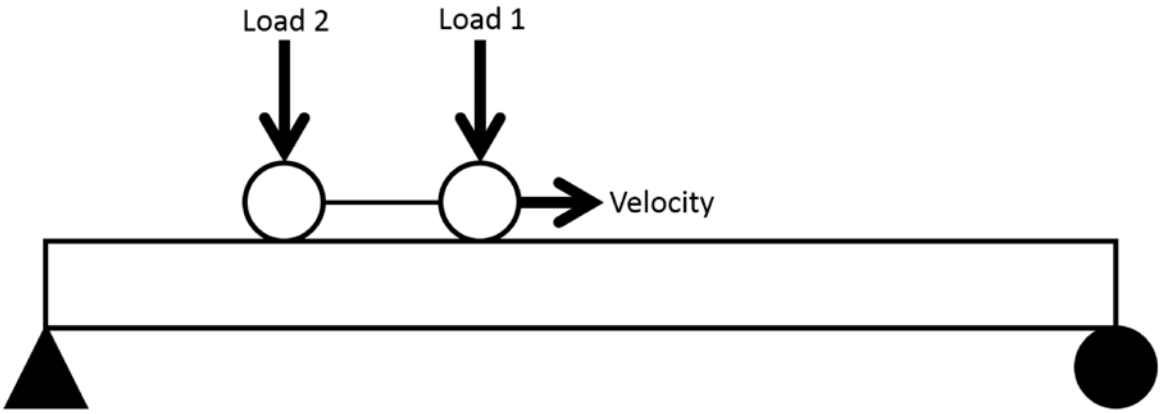

Fig. 3.3. Simply supported beam model with two point loads representing vehicle loads

To ensure the simulation is stable, a frequency of 1024 Hertz is used. Each load is applied sequentially to the intermediate (inter element) node points, preventing impact effects and providing a smooth movement of the point loads as they cross the beam. If the load application is too coarse, the movement is not smooth and it creates an unstable system. Silva's procedure only accounts for single axle vehicles crossing a beam [22]. Therefore, the approach was expanded here for multiple axle vehicles.

Figure 3.4 shows how a one ton moving point load moves through a 13 meter beam divided into 12 elements.

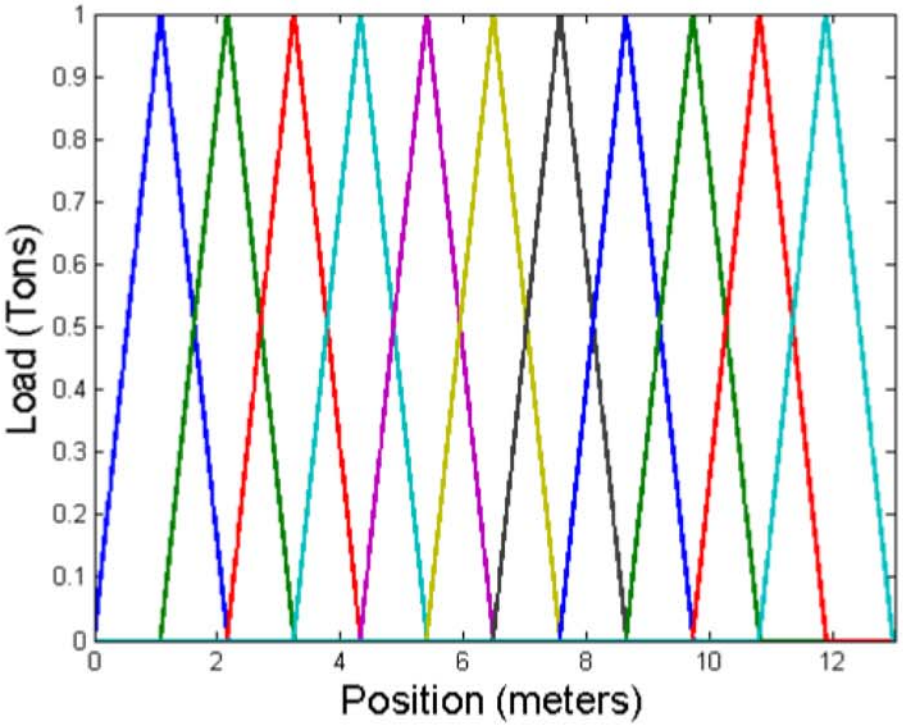

Fig. 3.4. Model of one wheel loading on a 12 element beam

As the load moves from one inter element node to another, the load increases to the maximum exactly over the node (1 ton), and then decreases smoothly to zero when it moves to another element. Figure 3.5 shows an example of a load between two nodes and equations and are the corresponding load values.

$$Load_A = \frac{L_e - l}{L_e} P \tag{3.23}$$

$$Load_B = \frac{l}{L_e} P \tag{3.24}$$

where l is the inter nodal length measured from node A, L_e is the length of the element, and P is the axle load. In the simulations, sometimes the axle length is shorter than

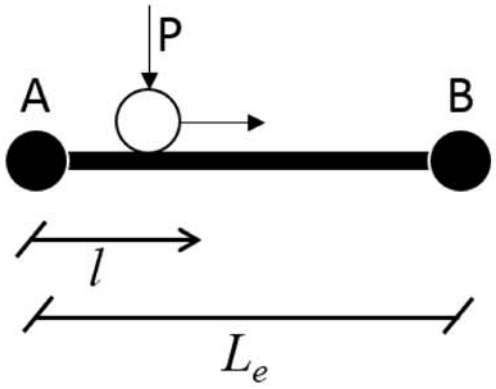

Fig. 3.5. Inter element loading example

the element length. Figure 3.6 shows a typical input vector for an MLC40, which has four axles. The double peaks shown occur because one of the axle lengths is shorter than the element length.

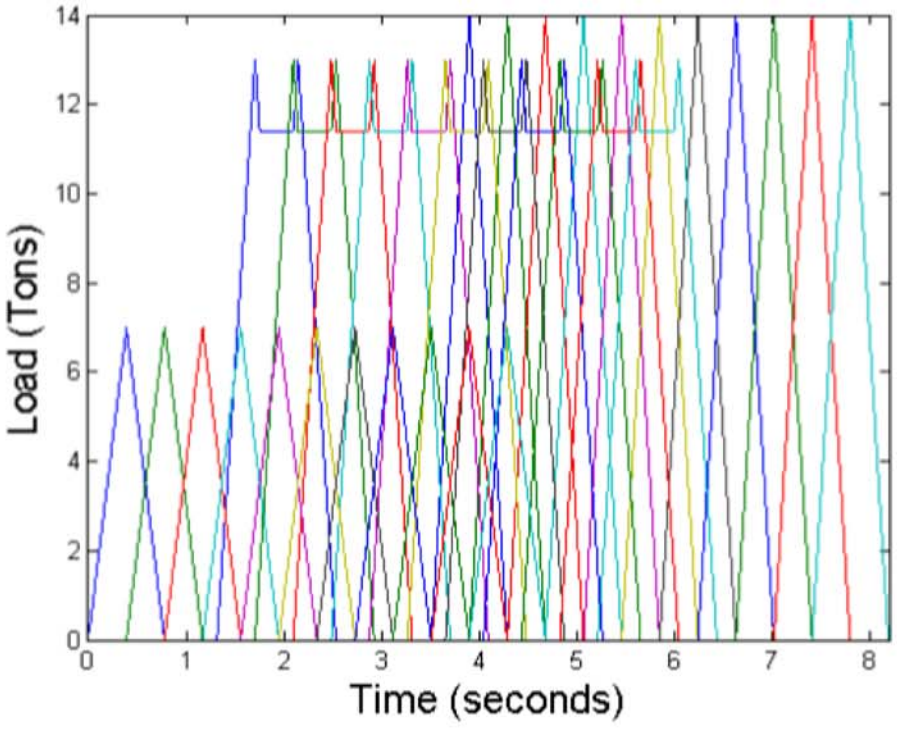

Fig. 3.6. Model of an MLC 40 loading on a 12 element beam

3.1.5 System Simulation

A linear simulation of the dynamic system created is performed using MATLAB. Figure 3.7 shows a representative mid-span acceleration response of the simulation. The simulation is performed for the time that the vehicle is on the bridge.

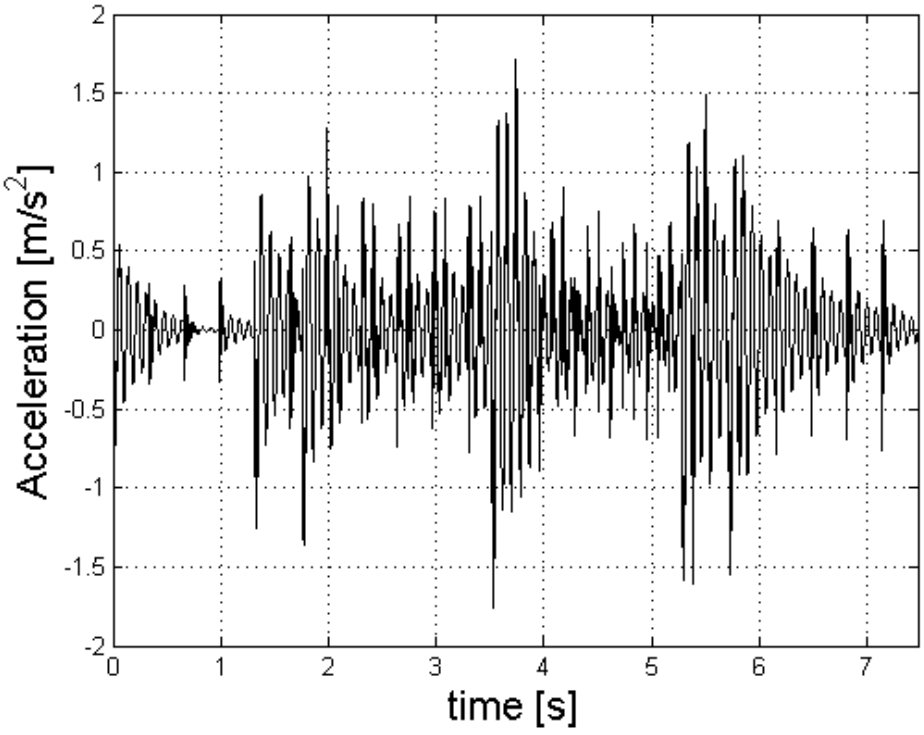

Fig. 3.7. Mid-span response of a 13 meter bridge due to MLC40 crossing at 15 km/hr

Once the response is obtained, it is then converted to a spectrogram, as explained in section 3.2.1. However, before conversion, noise is added when the analysis is considering noise in the sensors.

3.1.6 Adding Noise

The acceleration responses computed in the simulation are determined under a perfect setting. However, in every application noise exist. Therefore, the influence of noise on the performance of the method will be studied.

Noise is computed based on a percentage of the root mean square (RMS) of the response obtained. To compute the noise signal, $w(t_i)$, the following equation is used

$$w(t_i) = \beta_i * r * W(t) \tag{3.25}$$

where β_i is the i_{th} RMS value of the acceleration response, r is the noise ratio percentage in decimal value, and $W(t)$ is a uniformly distributed random process generated using MATLAB. Each noise signal computed is saved and added to the acceleration, as required. Figure 3.8 shows a 25% noise signal computed from the MLC 40 acceleration response shown in 3.7.

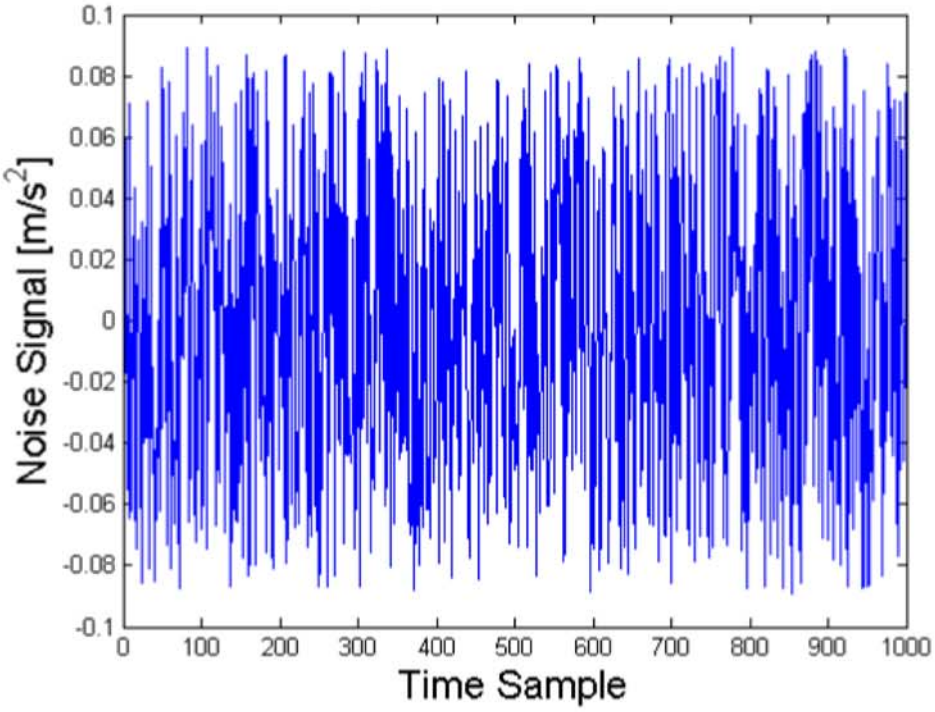

Fig. 3.8. Noise signal for an MLC 40 crossing response

3.2 Feature Detection Algorithm

Various computer vision algorithms have been developed to accurately identify a person or an object using the Viola-Jones object detection framework [12] [13] [30]. In this algorithm, computer vision principles are being applied to spectrograms, which are time-frequency visual representations of acceleration responses. Table 3.3 shows the algorithm that is used and the details of the procedure followed here.

Table 3.3.
Feature detection algorithm steps

Step	Description
1	Acceleration response is obtained
2	Accelerations converted to spectrograms
3	Integral images calculated
4	Haar features extracted from spectrograms
5	Gentle boost learning algorithm obtains strong classifiers
6	Classifiers are computed and stored
7	New vehicles cross and steps 1-5 are repeated
8	New vehicles are classified using the training classifiers and stored

3.2.1 Spectrograms

Spectrograms provide a visual representation of an acceleration response once a vehicle crosses a bridge. This allows the extraction of distinguishable features for classification. In the proposed procedure, the acceleration data is expected to begin when a vehicle enters the bridge and to stop when the vehicle exits, using strictly the response of the bridge while a vehicle is crossing. Thus, in the numerical investigations, the simulation response is restricted to the time while a vehicle is crossing the

bridge. However, in the experimental section, cropping had to be addressed to ensure the data is representative to the expected REB application.

Cropping and spectrogram creation are addressed in three steps. Step 1 is to acquire vertical acceleration signals from sensor nodes when the vehicle is traversing a mobile bridge. All sensors are triggered simultaneously when a vehicle enters the bridge. There are a number of techniques available to detect true event signals and differentiate them from noise, such as a STA/LTA (short term average/long term average) ratio method or threshold triggering [31]. The basic idea behind such methods is to capture sudden amplitude changes (increase/decrease) or fluctuations. These large changes/fluctuations do not typically occur in noise. In general, a vehicle entry event produces large accelerations similar to an impact load and the change can easily be distinguished. Thus, such methods are effective and applicable for our purpose.

Step 2 is to estimate the time at which the vehicle exits the bridge. The acceleration record to be used for classification should only contain data acquired when a vehicle is traversing the bridge. In general, the triggering algorithms used in step 1 can be applied in reverse to stop (exit triggering) recording data in the sensors. However, if the sudden exit of a vehicle acts as a large impact (releasing) force on the bridge and produce transient vibration, it would be difficult to estimate the time a vehicle exits using a simple amplitude-based threshold triggering method. Figure 3.9(a) presents a typical signal acquired in step 1 collected from the laboratory scaled experiment in Section 5.2. Unlike the sudden jump at the entrance of the vehicle, the response gently decreases at the exit.

To address this issue, we use the fact that the transient vibration is determined by the bridges dynamic characteristics, which are mainly composed of low frequencies. A high-pass filter is implemented to filter out the transient vibration of the bridge and retain the high-frequency components induced by vehicle crossing and noise. This process enhances the transition from a valid signal (the vehicle is on the bridge) to noise (the vehicle has exited the bridge) by reducing the free vibration of the bridge due to an impact load resulting from a vehicle exit. With this filter in place, the

triggering methods used in step 1 are applied to the filtered signals in reverse order to identify the exit time. In this study, a threshold triggering method is used to identify the exit time, and its threshold is estimated based on the background noise floor, which is measured with ambient conditions. In the threshold computation, the noise signals are assumed to follow Gaussian distribution with a zero mean and standard deviation of σ, the threshold limits are set to plus or minus $\mu\sigma$, where μ is a scaling factor and typically set to above 3.

Figure 3.9(b) represents the signal in Figure 3.9(a) after a high-pass filter has been applied. The boundary between the valid signal and noise is much clearer than in the record in Figure 3.9(a). The red dotted line denotes the estimated exit time using this reversed threshold triggering method. Note that the filtered signal is only used for determination of the exit time and cropping the original signal.

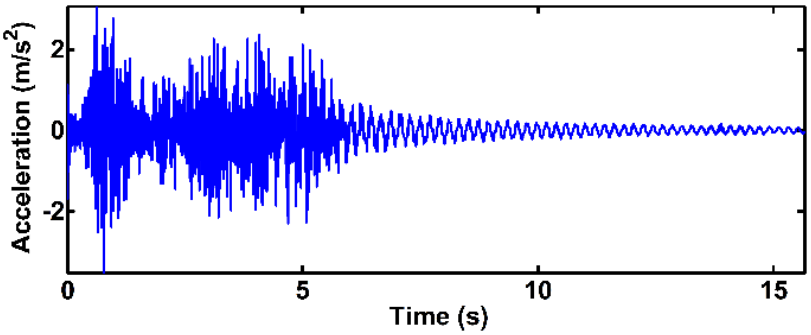

(a) Raw signal in step 1

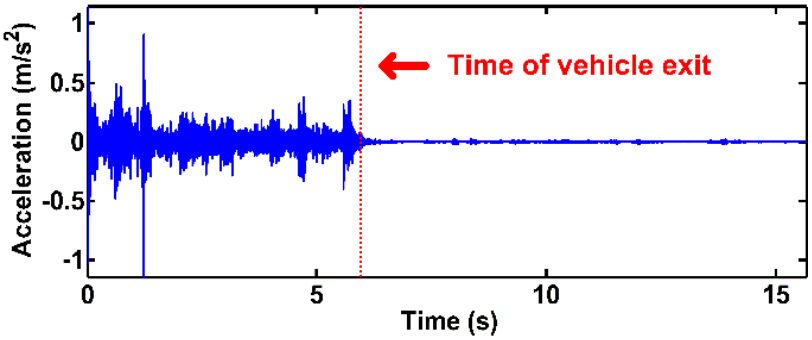

(b) Applying a high-pass filter for estimating vehicle exit time in step 2

Fig. 3.9. Acceleration cropping procedure (from [30])

The final step 3 is to transform the valid acceleration signals obtained using the entrance and exit times into spectrogram images normalized in size and scale. All images have the same number of points in the x (time) and y (frequency) axis, and a same spectral lines and frequency resolution. Suppose that all original signals are measured with the same sampling frequency using the sensors installed on the bridge. The sampling frequency should be determined based on the frequency bandwidth of interest. For simplicity, the number of time points in the spectrogram images is set to be higher than the maximum expected number of time points. This approach is used because down sampling will result in aliasing. Applying a low-pass filter in advance to prevent aliasing is not applicable in this case because a low-pass filter changes the frequency content in the signal and thus changes the spectrogram, making it difficult to compare the features in the spectrogram for classification. Note that the time resolution of the spectrogram image is also varied depending on the overlap of the Fast Fourier transform (FFT) frame. In this study, the FFT frame moves forward one time point at a time, and it produces same number of time points with time signals.

Spectrograms are computed from original signals with the same number of points in the FFT and two different sizes of frames. The frame lengths of the short-time Fourier transform for spectrogram conversion vary by resolution in both time and frequency. Good resolution cannot be achieved in both time and frequency with only one frame size. Thus, in this study, the spectrogram image is constructed with two spectrogram transformations using two different sizes of frames, and extracting features from appropriate time and frequency resolutions, respectively. Features used for classification will be extracted from both images, as discussed in the section 3.2.2.

The spectrograms generated from all original signals have the same frequency values along the y axis, but are not still consistent along the time axis due to variations in the speed. To correct this inconsistency, all spectrogram images are resized to have the same number of points along the x (time) axis. Figure 3.10 presents spectrogram images generated with the signal in Figure 3.9(a) after extracting the valid acceleration record. Each portion of the combined image has either better time or frequency

resolution depending on frame size used for spectrogram. Each portion of the image has been normalized here for visual clarity in this explanation.

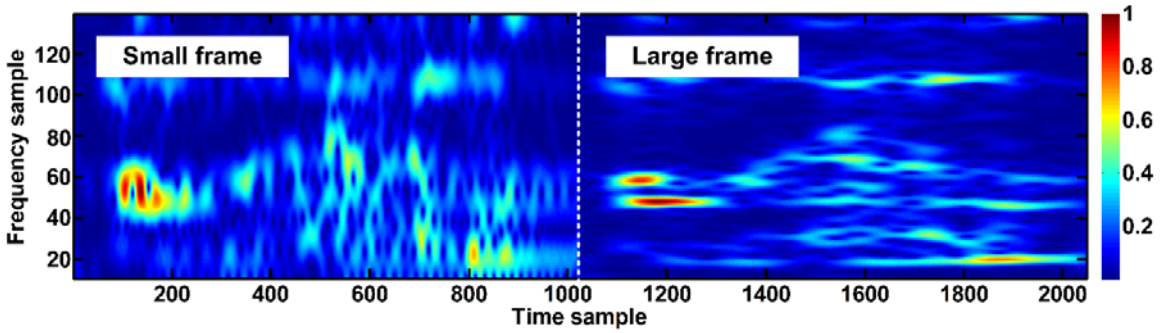

Fig. 3.10. Small and large frame window spectrograms

Now that the spectrograms are created, the main algorithm framework is used.

3.2.2 Viola-Jones Algorithm Framework

The Viola-Jones algorithm applied can be summarized in three steps: computation of integral image, extraction of Haar features, and application of the gentle boost learning algorithm. These steps are performed for both the training and testing phase.

Integral image is a step commonly utilized to compute an image's shaded pixel values fast without requiring major computational power [23]. It permits the evaluation of features quickly [12] when the Haar-like features are extracted from the image. Figure 3.11 shows a representation of how the integral image is computed, influenced by [32], where the value at a specific pixel is the sum of the pixels above and to the left of it.

Haar-like features are a set of clear and dark rectangles that are used to find strong features in an image [32]. Since the spectrograms produced do not have complex features, six types of simple rectangular Haar-like features suffice [12] [30], as shown in Figure 3.12.

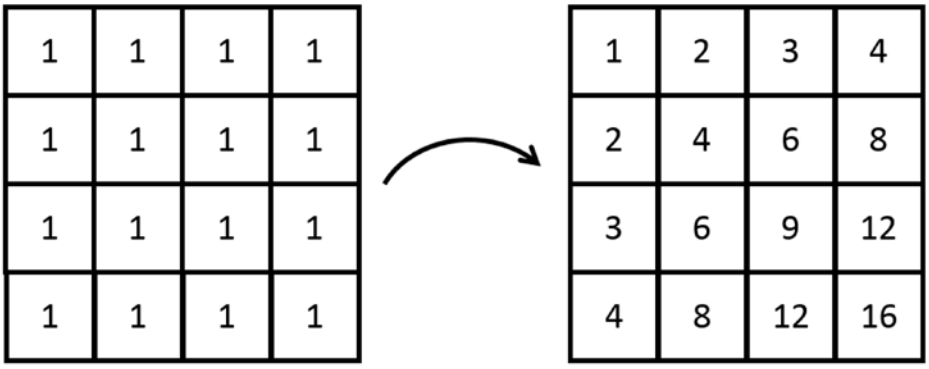

Fig. 3.11. Sample input image converted to integral image

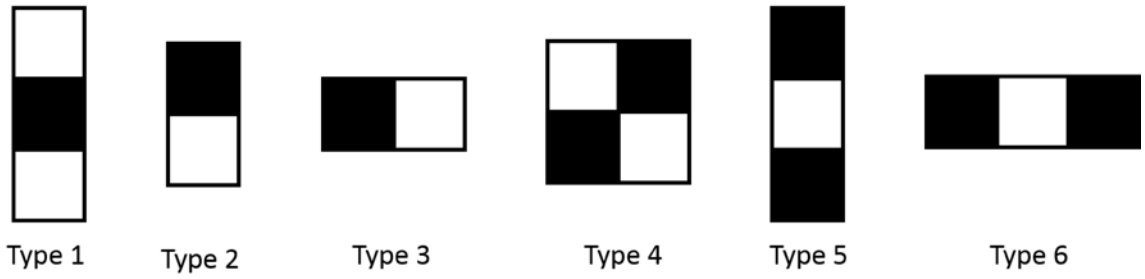

Fig. 3.12. Haar features used

These features allow the algorithm to numerically classify the image and quantify its contents, via distinguishable characteristics. Thus, Haar-like features are used to best fit the pixels of strong features of an image. Figure 3.13 shows a possible Haar-like feature extraction in a spectrogram image.

Every time Haar-like features are extracted, a numerical value is obtained based on the feature area of the dark and clear rectangles obtained from the pixels [32], as follows

$$Haar\ feature\ value\ = \sum(dark\ pixels\ ) - \sum(clear\ pixels\ ) \tag{3.26}$$

Haar feature values are computed from the most distinguishable features that are extracted in each round. The images produced will have thousands of features, but

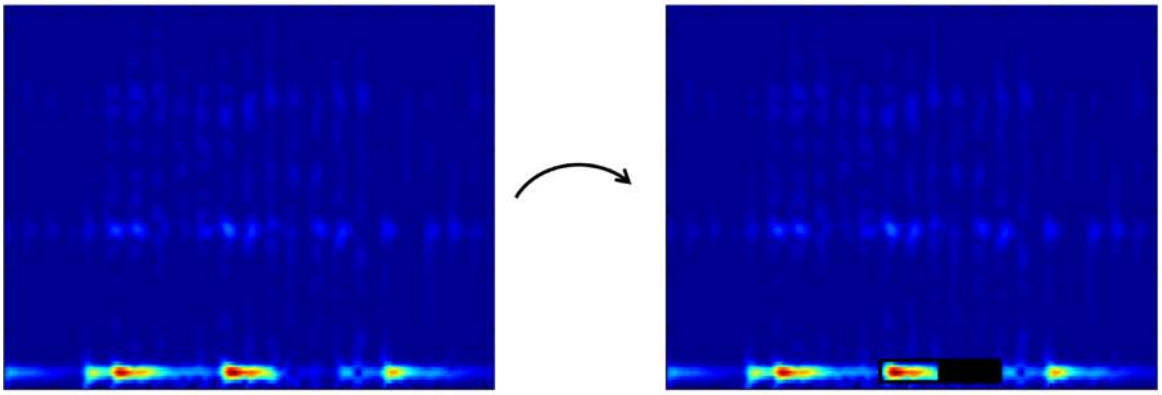

Fig. 3.13. Example of one Haar-like feature extraction

not all are important. Using the extracted values, these features can be reduced using a boosting algorithm. In this thesis, the gentle boost is used due to its simple application, numerical robustness, and experimental validation [33] [34].

Boosting first extracts weak classifiers. These classifiers are then weighted adaptively to reduce misclassification errors. Adaptively refers to updating the values of features based on prior results, thus highlighting stronger features and removing weak features from consideration. Once weighted, they are summed to create the most favorable strong classifier. These concepts are summarized in the equation below.

$$F_i(x) = \sum_{j=1}^{n} \alpha_j f_j(x) \tag{3.27}$$

where $F_i(x)$ is the i_{th} round strong classifier, α_i is the weight of the j_th weak classifier, $f_j(x)$ is the j_{th} weak classifier or strong feature detected, and n is the number of rounds. A round is when a specific region of the image features is extracted and computed to create weak classifiers, which then compose the strong classifier for the round, as shown in equation 3.27. As additional rounds are conducted, the region evaluated changes based on the most distinct features. Thus, a new strong classifier is calculated every round. As each round occurs, the weight of the weak classifiers changes adaptively to reduce misclassification, helping to select the best region to

evaluate. A visual depiction of how classifiers are selected and weighted per round is shown in Figure 3.14, influenced by [32].

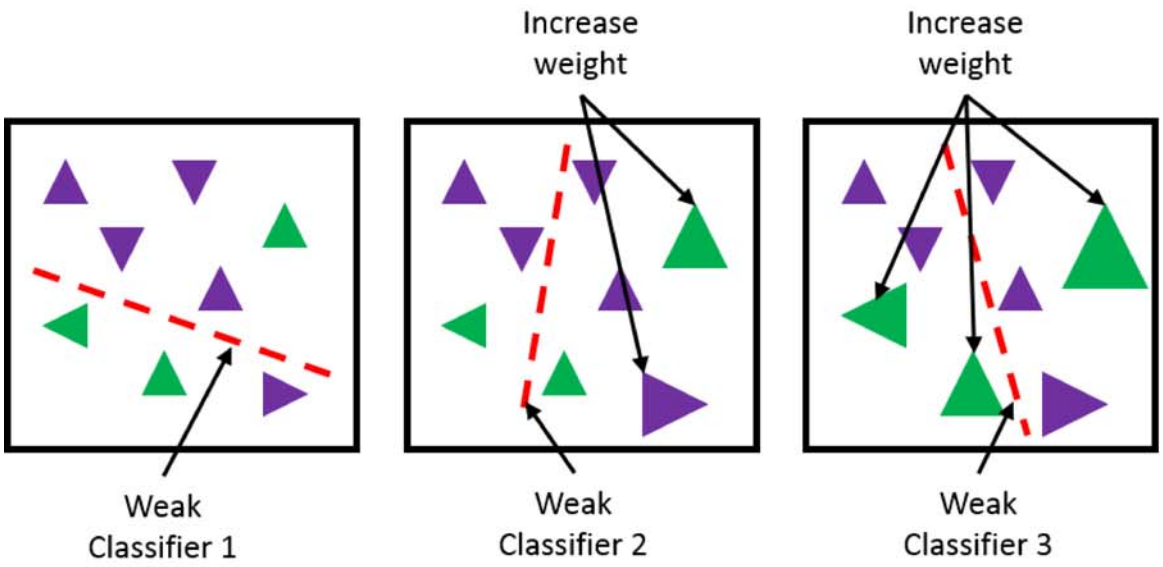

Fig. 3.14. Strong classifier representation

In this investigation, 50 rounds are conducted for the numerical tests and 100 rounds for the experimental tests, to obtain 50 and 100 strong classifiers per image, respectively. These classifiers are saved for future vehicle classification.

For example, when a new spectrogram is compared to the training spectrogram, the same 50 rounds will be applied. Each round, the new testing strong classifier is compared to the saved training strong classifier and if they match, it yields a value of 1. However, if they do not match, it yields a value of -1. Additionally, if part of the strong classifier matches but other do not, then the value will be somewhere in between -1 and 1. Since there are 50 rounds, a complete perfect match will yield a total value of 50, a complete mismatch will yield a value of -50, and partial matching will yield a value between -50 and 50.

For classification problems, one versus rest (OvR) and one versus one (OvO) can be applied. In this study, OvO is adopted because it heuristically provides better classification outcomes, as recommended by Yeum [30].

These classifiers can be trained individually or correlated. Individual training is used in the numerical investigation, section 4, because only one acceleration response per crossing is obtained for training. Correlated training occurs in the experimental validation, section 5, because multiple accelerometers are used and there is a relationship between the responses. Once the algorithm is applied, results obtained are discussed in the form of a confusion matrix.

3.2.3 Confusion Matrix

The confusion matrix is commonly used to demonstrate the results of supervised learning algorithms [35]. As shown in figure 3.15, the rows refer to the actual class while the column refers to the predicted class. If both the actual and predicted class match, it is considered to be a perfect classification. If they do not match, then it is seen how the actual class was misclassified by reading the predicted class. For example, it can be seen that Class 4 was misclassified as Class 3 two times.

		Predicted										
		1	**2**	**3**	**4**	**5**	**6**	**7**	**8**	**9**	**TOTAL**	**% per class**
Actual	**1**	25	0	0	0	0	0	0	0	0	25	100.0
	2	0	25	0	0	0	0	0	0	0	25	100.0
	3	0	0	23	0	2	0	0	0	0	25	92.0
	4	0	0	2	21	2	0	0	0	0	25	84.0
	5	0	0	5	0	17	3	0	0	0	25	68.0
	6	0	0	1	0	3	21	0	0	0	25	84.0
	7	0	0	0	0	0	0	25	0	0	25	100.0
	8	0	0	0	0	0	0	0	25	0	25	100.0
	9	0	0	0	0	0	0	0	2	23	25	92.0

Fig. 3.15. Confusion matrix results example

Confusion matrices allow for rapid assessment of misclassification occurs and the overall performance of the method. It provides insights into similar strong features pattern across classes.

3.3 Summary

This background chapter provides an explanation of the procedures used to develop a finite element model that provides acceleration results, and a description of how the acceleration results from both the finite element model and experimental results are converted to spectrograms and taken through the feature detection algorithm. Results will be summarized in confusion matrix form for analysis.

4. NUMERICAL INVESTIGATION

To assess the sensitivity of the results due to variations in parameters, a finite element model [22] is used to obtain acceleration responses and analyze them with the feature detection algorithm. The finite element model creation is explained in section 3.1. Numerical experiments provide a thorough study of various parameters at little to no cost. It also provides guidance in how to properly conduct field experiments.

4.1 Simulation Explanation

The simulation code is built so the user can vary the following parameters: bridge length, vehicle speed, noise, vehicle loading, sensor filter and material properties. In all cases, the material properties are kept constant, as recommended by Silva [22]. The bridge is modeled as a simply supported homogeneous beam, as it closely mirrors the real world emplacement guidelines [7].

The model is developed to have similar dynamic characteristics to the REB. As explained by Silva [22], steps are followed to reach dynamic behavior equivalence. First, a finite element model is defined with specific material properties. Second, a modal analysis of the REB is conducted to determine the natural frequencies of the bridge for the first three modes. Third, the inertia and stiffness parameters of the numerical model are updated until the frequencies closely match the ones obtained in the REB. Finally, the material properties are set and the numerical model can be applied to various parameters and loading conditions.

Acceleration responses can be obtained at any specific location and are generated at a sampling frequency of 1024 Hertz. However, the mid-span acceleration is the only response used for all training and testing, closely matching the actual procedure intended by the user. Once the response is obtained, it is passed through a filter with

a cut-off frequency of 60 Hertz and re-sampled to a data rate of 120 Hertz. This same procedure will later be conducted in the field experiments described in section 5.

The bridge should be examined under a variety of setups and conditions, which can be cost prohibitive for field experimentation. Therefore, the following numerical study provides the results to guide future experimental studies and to develop a general bridge procedure. The end goal is to determine which parameter changes yield more variation in the results and how to develop an implementation procedure.

The following simulations will consider different variations in sensor filter, bridge length, speed and noise at different levels. These parameters are key to understanding the capabilities of the algorithm and how to use if effectively with successful outcomes.

4.2 Vehicle Loadings and Classes

The vehicles used for the simulation are the hypothetical MLC. The MLC were created by the military in order to correlate all types of vehicles, tracked and wheeled, into one common type and also determine the maximum class a bridge can support [36]. For example, an MLC 4 is a vehicle of approximately four short-tons, or 3,628 kilograms. Existing guidance, outlined in the Engineer Reconnaissance Field Manual [37], can convert any existing vehicle into an MLC. Some common vehicle classifications are shown in Table 4.1.

Table 4.1.
MLC vehicles (from [37])

MLC	**Vehicle**
4	High Mobility Multipurpose Wheeled Vehicle (HMMWV)
12	Backhoe
20	Mine Resistant Armored Protected (MRAP) Truck
40	D7G Mine Clearing Bulldozer with armor
50	M870 semi trailer

The REB manual indicates the heaviest vehicle allowed is an MLC 50 [7]. Therefore, simulations are conducted for nine MLC, from MLC 4 to MLC 50. Initially, MLC are studied, but alternative groupings are considered based on the needs of the user and the success of the algorithm. Figure 4.1 shows the trend after a simulation in Confusion matrix form. The red color shows the under classification and the yellow shows over classification.

		Predicted									
		Class 1	Class 2	Class 3	Class 4	Class 5	Class 6	Class 7	Class 8	Class 9	% per class
Actual	Class 1	58	0	0	0	0	0	0	0	0	100.0
	Class 2	0	35	0	0	0	0	0	0	0	100.0
	Class 3	0	0	16	6	6	13	3	1	0	35.6
	Class 4	0	0	5	27	16	5	0	0	0	50.9
	Class 5	0	0	5	17	10	1	0	0	0	30.3
	Class 6	0	0	17	4	11	17	1	1	0	33.3
	Class 7	0	0	4	0	1	1	47	0	0	88.7
	Class 8	0	0	0	0	0	0	0	34	3	91.9
	Class 9	0	0	0	0	0	0	0	6	34	85.0
									Detecton Rate		72.8

Fig. 4.1. Typical simulation results

Under classification and over classification occurs when a vehicle lighter and heavier, respectively, than the actual is classified. Over classification is preferred to under classification, as it is conservative. Trends show unique responses related directly to the axle length of vehicles, spreading classification into three groups. MLC 4 to 8, 12 to 30, and 40 to 50 have equal or similar axle lengths. Therefore, the nine individual MLC indices are assigned to three groups based on similar axle lengths. Table 4.2 shows the indexing of the classes and groups.

Table 4.2.
MLC individual and group indices

Actual MLC	Individual Index	Group Index
4	1	1
8	2	1
12	3	2
16	4	2
20	5	2
24	6	2
30	7	2
40	8	3
50	9	3

4.3 Sensitivity Study

The sensitivity study is intended to determine how to implement the algorithm and design the training to improve the accuracy of the feature detection algorithm under varying parameters. Sensitivity refers to the degree that the algorithm results are affected by parameter variation. The goal is to increase the accuracy for both individual and group indexes to a rate above 90 percent.

The following simulation numbers are implemented for all cases studied: 100 simulations per individual MLC, 75 for training and 25 for testing, for a total of 900 simulations, 675 training and 225 testing. All studies are divided into four general cases. Cases 1 and 2 reflect the perfect laboratory scenarios, where the training and testing occur at identical noise level. Cases 3 and 4 present the more realistic scenarios, where the noise level differ for training and testing. For all cases, an additional letter will be added to the end of the case number to explain which parameter is

studied. For example, Case 1F refers to Case 1 for the filter parameter. For cases in this study, F means filter, L means length, S means speed and N means noise.

4.3.1 Accelerometer filter

The accelerometer currently expected to be available by the user allows a low pass filter setting of either quarter or half data rate. This setting can help capture the distinct features that are created when vehicles cross. This is especially important due its low sampling frequency of 120 Hertz. To determine the best setting among these options, three filtering variations are studied in this section: none, quarter data rate, and half data rate.

For all simulations, the length of the bridge will be random, and is uniformly distributed from 8 to 12 meters, speed is set to 15 km/hr and vehicle load varies less than 5%. A total of 60 simulations are conducted, 20 per filter setting. It is assumed that the user will not change the filter setting between training and testing environments, as it will present additional calibration and time issues. The four cases studied are summarized below:

Case 1F	Training and testing without noise
Case 2F	Training with 5% noise and testing without additional noise
Case 3F	Training without noise and testing with 5% to 40% additional noise
Case 4F	Training with 5% noise and testing with 5% to 40% additional noise

Group index detection results are very similar, regardless of the filtering level. 98% detection rate is achieved in case 1F and 100% in cases 2F, 3F, and 4F. The algorithm is not sensitive to the filtering level when group indexes are used. Individual indices shed light into what filter level is better.

In individual MLC detection, the training and testing data for all 60 cases demonstrated that no filter provides the worst accuracy. Therefore, it will not be considered

nor discussed. In cases 3F and 4F, which vary the noise added for testing, half data rate filtering provided better results on 70%, 14 out of 20, of the total simulations. The results for 3F and 4F can be seen in Figure 4.2.

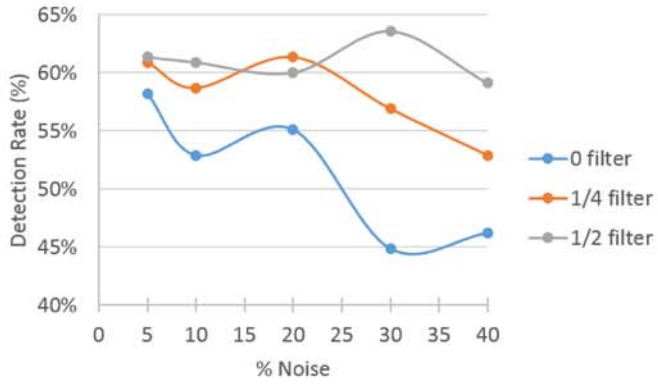

(a) Case 3F

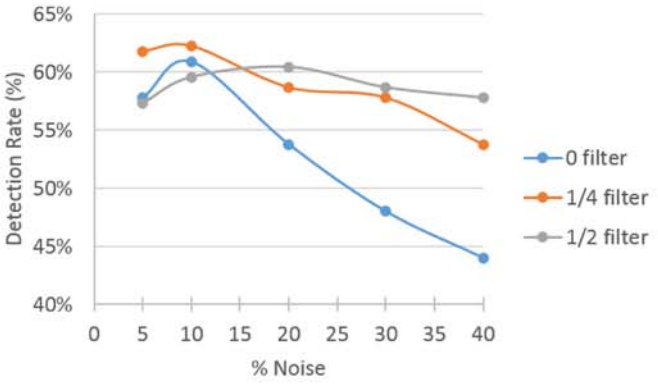

(b) Case 4F

Fig. 4.2. Sensor filter detection rates

When training and testing occurs at the same filter level, some filtering is better than none for individual index classification. Overall, the half data rate filter consistently provides better results than quarter data rate, and is the recommended filter setting for the experiment and likely, for the implementation. The rest of the study is conducted using half data rate filter in order to acquire the best results possible for both indexes.

4.3.2 Length variation

The REB can be placed over any span up to a maximum length of 13 meters [7]. In real world applications, span variations affect bridge properties and behavior. It is important to study how the difference between short and long span responses as well as the range of lengths in the training database affect results. Figure 4.3 demonstrates the challenge of visually comparing the same MLC crossing at different lengths. It is evident that they are quite different.

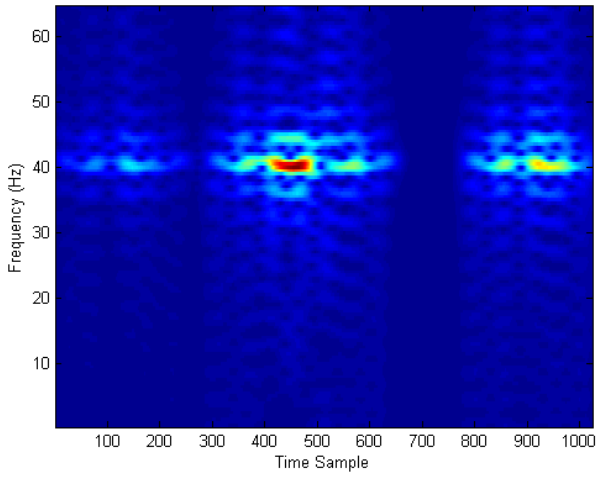

(a) 3 meter response

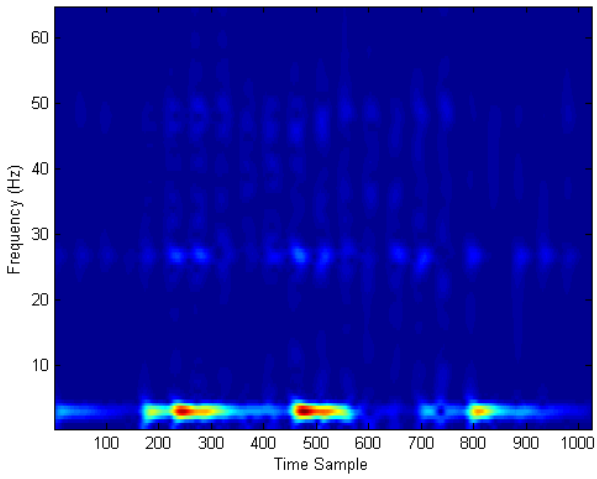

(b) 12 meter response

Fig. 4.3. MLC 40 acceleration responses at different lengths

In this parameter study, bridge length will be random and uniformly distributed from 2 to 13 meters, for all possible integer range combinations, including fixed lengths. Fixed lengths refers to using only one specified bridge length. Some combinations of the possible 78 are: 6 to 10, 2 to 13, and a fixed length of 10 meters. The following parameters remain constant throughout the study: vehicle load varies less than 5% and speed is set to 15 km/hr. Below are the four cases that are examined:

Case 1L Training and testing without noise

Case 2L Training with 5% noise and testing without additional noise

Case 3L Training without noise and testing with 10% additional noise

Case 4L Training with 5% noise and testing with 10% additional noise

Individual index results demonstrate that the detection rate increases as the length range gets smaller and closer to a fixed length, regardless of the case applied. This means that the worst rate classification results occur at the extremes, from 2 to 13 meters, while the best occur at fixed lengths. Figure 4.4(a), (b), and (c) shows how the smaller range produces better results for cases 3L and 4L. The detection rate on the ending length axis (x-axis) refer to the ending range. For example, Figure 4.4(b) case 3L shows a detection rate of approximately 60% at ending length 9 meters. This means that the bridge length range was selected at random by uniform distribution from 6 to 9 meters.

For individual index fixed length results, Figure 4.3(b) shows case 4L detection rate increased by an average 23% over case 3L, achieving a near perfect classification in the simulations. This demonstrates that noise training produces consistently better results when additional noise is added for testing. This scenario is closer to the field application, where the noise cannot be perfectly replicated in training and the testing noise is higher.

The best results occur when group indices are applied. Group index results demonstrate, for lengths 4 meters and above, that the detection rate increases as the length

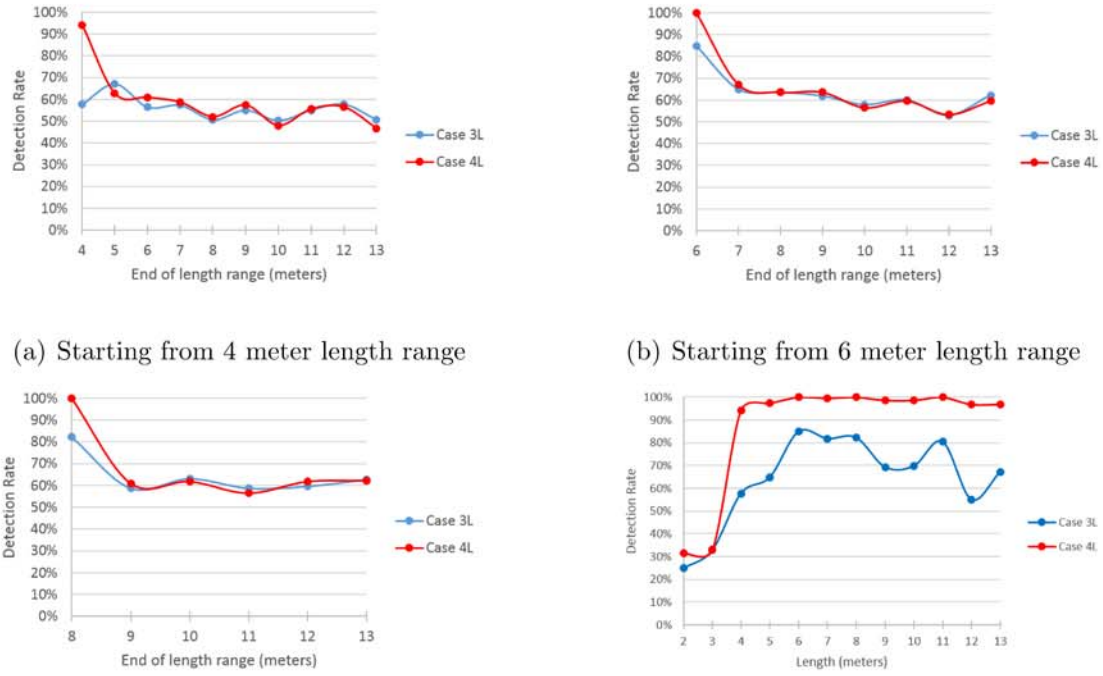

(a) Starting from 4 meter length range

(b) Starting from 6 meter length range

(c) Starting from 8 meter length range

(d) Fixed bridge lengths

Fig. 4.4. Cases 3L and 4L detection rates for bridge length ranges and fixed

range gets closer to a fixed length, regardless of the case applied. However, Case 3L and 4L produced a rate above 72% and 89%, respectively, for any length range that is not fixed. For fixed lengths from 4 to 13 meters, the results for case 4L are above 94%. These results show, yet again, that training with noise is consistently the better option. Although, at fixed spans of two and three meters, the detection rates are unsatisfactory for cases 3L and 4L, as shown in Table 4.3.

Short span classification results present a sensitivity issue. As the bridge span is shortened, its natural frequencies increase. These higher frequencies decrease the number of distinct features in the response and therefore, the strong classifier is harder to distinguish. As shown in Figure 4.3(a), which is a 3 meter span, strong features appear at approximately 40 Hertz at various time steps. Figure 4.3(b), which is a 12 meter span, shows strong features at approximately 4 Hertz and additional features at approximately 26 and 48 Hertz. Figure 4.3(a) does not appear to have as many

Table 4.3.
Detection rate at short spans (less than 4 meters)

Case	Fixed Length	Individual Rate	Group Rate
3L	2 meters	25%	63%
3L	3 meters	33%	74%
4L	2 meters	32%	66%
4L	3 meters	33%	73%

distinct features as Figure 4.3(b), which leads to misclassification due to the limited number of unique features across classes.

The limitations imposed on the sensor sampling frequency make it difficult to accurately detect individual vehicles in short spans of 2 and 3 meters. Increasing the sampling frequency of the sensors may address this issue, but it should be further studied on future experiments. Within current guidelines, use of the group index provides a superior detection rate and can help offset the results sensitivity.

Despite having good results for individual indexes in fixed lengths 4 meters or above, it is infeasible to garner all possible length variations and ranges. Therefore, small length ranges should be considered for implementation. For example, if the training database has response data for integers between 3 and 13 meters, but the test occurs at 10.5 meters, then it will try to match to either 10 or 11 meters. Even though the response relationship is not linear, the detection probabilities increase at smaller ranges. In this type of case, the algorithm works best for cases 3L and 4L.

Remarks: This study highlighted what range of lengths are acceptable to accurately detect the right class of vehicle for both indexes. To acquire over 90% detection rate: training should be conducted with noise, group index provide overall best results, and length range should be as small as possible or known.

4.3.3 Speed Variation

The REB can be crossed at speeds up to 40 km/hr [7], but are typically crossed at 15 km/hr when ground guides are present. Speed is difficult to control in field applications, which may hinder accurate classification. Figure 4.5 shows an example of how the spectrogram varies when only the value of the constant speed is changed. It is visually evident that despite having distinct features at similar frequencies, certain features get stronger at higher speeds and this makes it difficult to compare them.

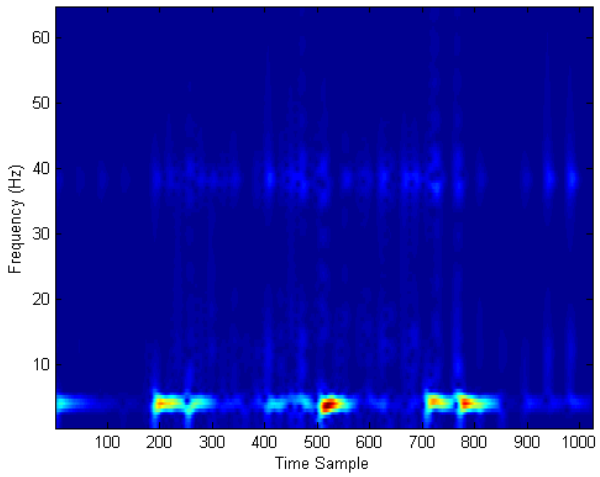

(a) 10km/hr Crossing

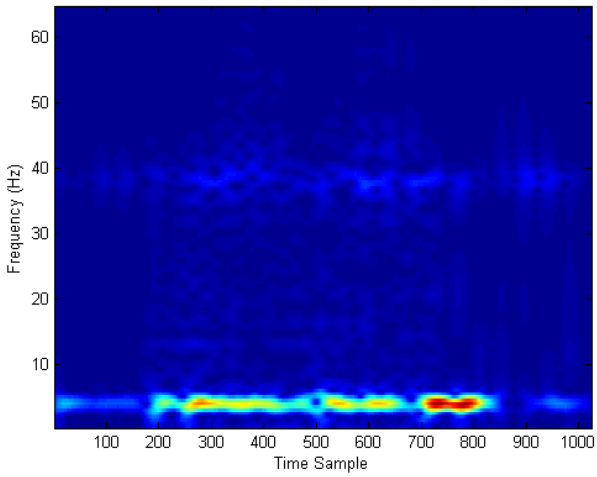

(b) 20km/hr Crossing

Fig. 4.5. MLC 40 acceleration responses at different speeds

The following parameters remain constant for this study: vehicle load varies less than 5% and length is fixed at integers from 2 to 13 meters. Speed variation will be random and normally distributed with a mean of $15km/hr$ and a σ of 3, 2, 1 and 1/2. Once the vehicle enters the bridge, the speed is assumed constant throughout, as the REB manual states that there should be no sudden acceleration during crossing [7]. 12 possible constant lengths and four speed variations are considered, for a total of 48 simulations. Below are the specific cases that will be considered:

Case 1S Training and testing without noise

Case 2S Training with 5% noise and testing without additional noise

Case 3S Training without noise and testing with 10% additional noise

Case 4S Training with 5% noise and testing with 10% additional noise

For both indices, the results generally show an increase in detection as σ decreases. The short span lengths, 2 and 3 meters, continue to yield lower detection rates, for reasons explained in section 4.3.2. Figure 4.6 shows the summary of results per speed variation for cases 3S and 4S in both indeces.

Individual index results in cases 3S and 4S averaged detection rates of 67% and 69%, respectively, with better 4S results 69% of the time. However, no results showed a rate over 90%. The best results where obtained in the groups. Group indexing results in cases 3S and 4S had detection rates above 92% and 97%, respectively, for lengths higher than 4 meters at all σ variations. Even at 3 meters, 3S and 4S resulted in rates above 85% and 95%, respectively. When group indexing is applied, speed variation up to a $\sigma = 3$ does not affect the detection rate considerably.

In field scenarios, speed will always vary from vehicle to vehicle, depending on the driver. If the speed is controlled up to a maximum $\sigma = 3$, which provides a range of plus or minus $5km/hr$, then the detection rate will not be affected when group indexing is applied. Speed can be controlled by ground guides or maximum and minimum speed signs.

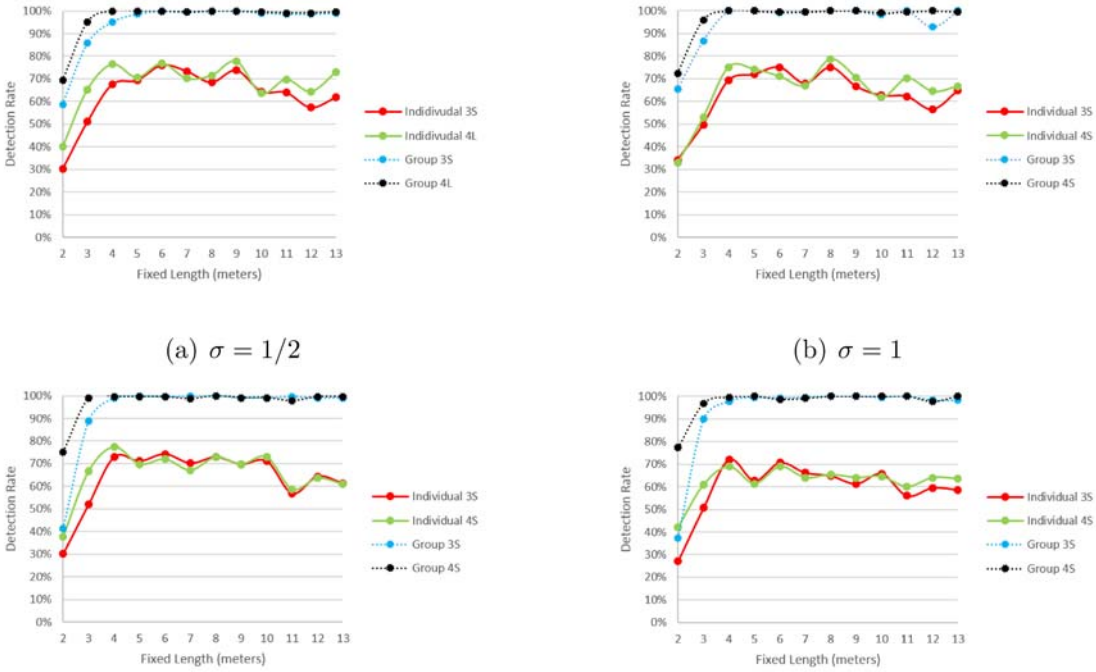

(a) $\sigma = 1/2$ (b) $\sigma = 1$

(c) $\sigma = 2$ (d) $\sigma = 3$

Fig. 4.6. Fixed length detection rate at different σ

4.3.4 Noise Variation

The REB is to be employed in an amalgam of conditions for which noise can only be estimated. Since noise levels will vary greatly, it will be impossible to predict and model all possible outcomes. Figure 4.7 shows how a variation of noise can change the spectrogram plot and make it difficult to compare. It shows how additional distinct features appear at higher modes.

In order to study the sensitivity of the algorithm to additional noise during the testing phase, training occurred without noise and with 5% noise. No noise training relates to perfect conditions while 5% noise training relates to normal operating conditions. The 5% noise is determined using experimental data from section 5.2. The procedure for adding noise is explained in section 3.1.

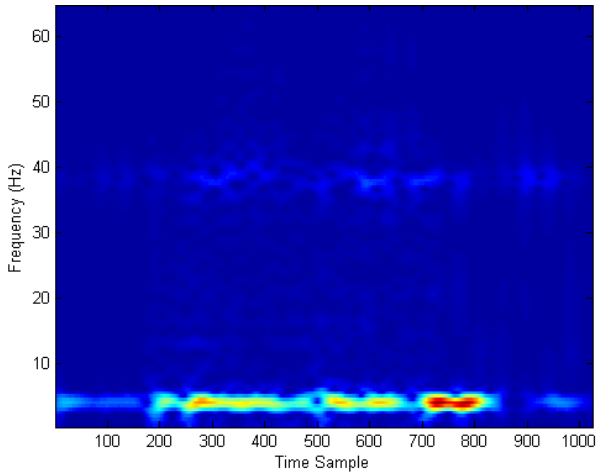

(a) 5% Noise

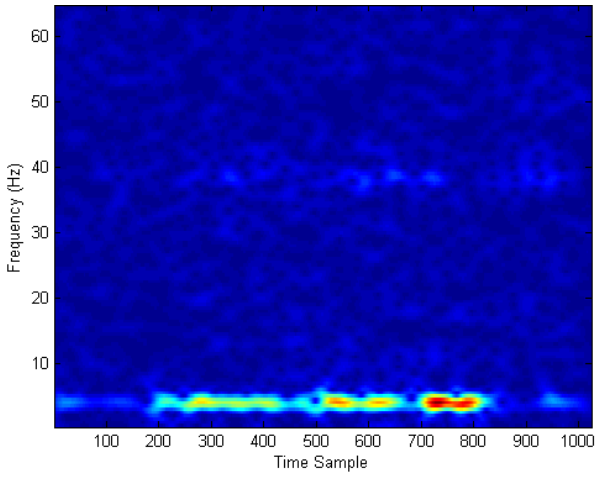

(b) 25% Noise

Fig. 4.7. MLC 40 acceleration response with different noise added

Simulations are also conducted at an additional noise of 5%, 10%, and 25%. The following parameters remain constant for this study: vehicle load varies less than 5%, speed is fixed at 15 km/hr, and length is fixed at integers from 3 to 13 meters. There are 11 possible fixed lengths and 3 additional noise parameters, for a total of 33 simulations. The specific cases that will be considered are shown below:

Case 1N Training and testing without noise

Case 2N Training with 5% noise and testing without additional noise

Case 3N Training without noise and testing with 5% to 25% additional noise

Case 4N Training with 5% noise and testing with 5% to 25% additional noise

The results show the lower the noise percentage added, the better the detection rates, as expected. A graphical summary of the results is shown in Figure 6.5.

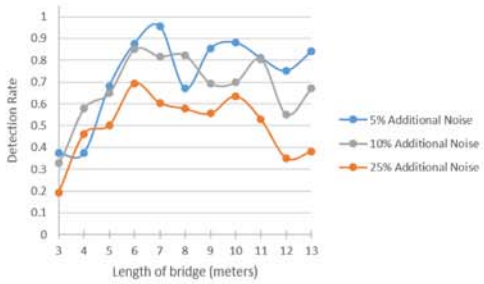

(a) Individual Index Case 3N

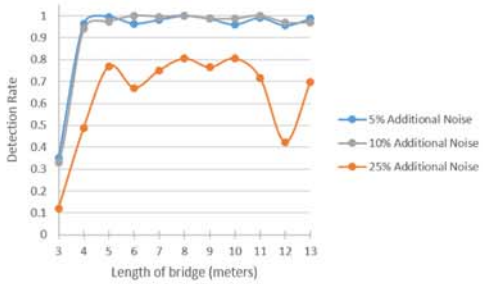

(b) Individual Index Case 4N

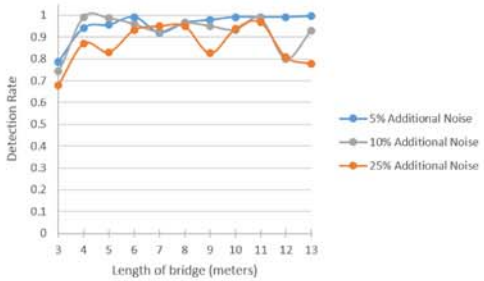

(c) Group Index Case 3N

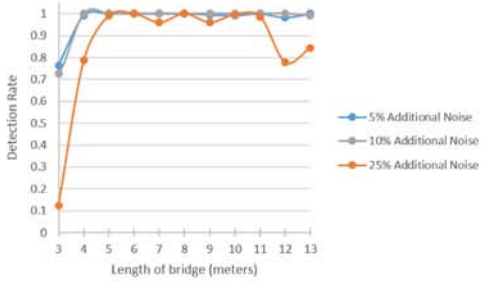

(d) Group Index Case 4N

Fig. 4.8. Detection Rates for Cases 3N and 4N

Individual index detection rates for case 3N are unacceptable and fluctuate heavily, as shown in Figure 6.5(a). In 3N, the only reasonable results, close to or over 90%, occur at 5% additional noise at fixed lengths 6, 7, 9, and 10 meters. Case 4N, shown in Figure 6.5(b), is superior to 3N with consistent good results over 90% at additional noise levels of 5% and 10% for fixed lengths between 4 and 13 meters.

The group index detection rates meet the stated requirements for cases 3N and 4N, Figures 6.5(c) and 6.5(d), respectively. However, 4N has overall better results. Additionally, case 4N obtains over 90% detection rate for an additional noise of 25% between 5 and 11 meters, which is five times the training noise level. The better detection rate of case 4N provides expanded capabilities to the algorithm in relation to noise. Low detection rates are captured for the short three meter length case, for reasons explained earlier in section 4.3.2.

Remarks: The noise parameter study highlights that when training occurs with noise, additional noise can be tolerated and still produce a group index detection rate above 90%. The most realistic training scenario should be applied when collecting the training data and no additional noise scenarios are required, given the tolerance of the algorithm to noise. Therefore, noise is considered a low sensitivity parameter and does not present much concern, as long as the training occurs in a representative environment and the additional noise during testing is not too high.

4.4 Implementation Recommendations

The numerical investigations included in this chapter demonstrate that the algorithm results are most sensitive, in order of impact, to: bridge length, vehicle speed, noise, and filter. Knowing or controlling these parameters will help the user obtain the required detection rate. Recommendations are compiled in Table 4.4 for field implementation.

These recommendations tend to produce the best environment possible for reliable detection rates. They serve as a starting point for a future thorough study of the REB, under the various conditions stated above.

Table 4.4.
Best Parameter Settings

Parameter	**Recommendation**
Sensor filter	Half data rate setting
Bridge length	Compile integer lengths from 3 to 13 meters
Speed	Control speed plus or minus $5km/hr$
Noise	Train with realistic field conditions
Index	Group

It is important to note that the group index classification developed was based on vehicle axle length and the limitations of the model created. The model does not account for the dynamic interaction between the bridge and the vehicle, which occurs in the real world. Thus, the lack of individual classification can also be attributed to the limitation of the model.

5. EXPERIMENTAL VALIDATION

Experimental validation is conducted to demonstrate the premise that each vehicle class will produce a distinct acceleration response, allowing identification under the algorithm developed. Validation is explored in two separate experiments: a full scale mobile bridge and a laboratory scale bridge. These experiments aid in demonstrating the initial capacity of the algorithm, provide insights in the results sensitivity to parameters, and guide implementation recommendations.

The experiments are conducted under the following similar parameters and procedures. Data acquisition occurs at a sampling frequency of 1024 Hertz with an accelerometer PCB model 333B40 [38]. An m+p VibPilot data acquisition system is used with a 24-bit analog to digital converters, simultaneous sample and hold, and built-in anti-aliasing filters linked to the sampling rate [39]. Since the algorithm is expecting data acquired at 120 Hertz, the original response is passed through a low pass Butterworth filter with a cut-off frequency of 60 Hertz and re-sampled to a data rate of 120 Hertz . This reduction in data helps mirror the expected spectrograms that will be constructed by the user. Once the acceleration data is obtained, a spectrogram will be created with a Hanning window of 32 and 128 frame sizes, small and large window, respectively [30]. Then, 20,000 features are created for each spectrogram, where a strong classifier will be composed of 100 weak classifiers [34]. Training and testing will occur under various conditions, depending on the experiment and the data.

Correlation classification is applied to the experimental results because of the use of multiple accelerometers. In the REB and scaled experiments there are 12 and 8 responses obtained, respectively. The accelerometers are located along the length of the mobile bridges and a match of at least 75% is used for correct classification.

Correlation is preferred to individual classification as it takes into account the response of the mobile bridges at different locations and the relationships between them.

5.1 REB Experiment

The full scale bridge experiment is conducted on the REB. This experiment demonstrates the use of the vehicle classification algorithm with actual acceleration responses, illustrates the occurrence of distinct features between vehicles, and provides guidance on how to conduct the laboratory scale experiment. REB tests were intended to be extensive but, limited amount of time was available for testing due to reason beyond our control.

5.1.1 Setup

The bridge is set up and crossed by two vehicles under a specific set of parameters, shown in Table 5.1. The two vehicles, a small Sport Utility Vehicle (SUV) and a small pickup truck, Vehicles 1 and 2, respectively, produce acceleration responses that are measured as they cross.

Table 5.1.
REB experiment parameters

Parameter	**Explanation**
Bridge Length	Approximately 13 meters
Vehicle Speed	4, 6, and 9 km/hr
Setup	Wood supports on grass surface

Vehicle 1 crosses the bridge five times at each speed mentioned in Table 5.1, for 15 crossings. Vehicle 2 crosses the bridge four times at each (4 and 9 km/hr) speed, for a total of 8 crossings. Thus, there are 23 total crossings. 12 accelerometers, six per

side, are installed along the length of the bridge to capture each crossing acceleration response. Figure 5.2 shows the main bridge setup with the sensor locations.

(a) Sensor locations

(b) Sensor close-up on REB top flange

(c) Isometric view (from [30])

Fig. 5.1. REB experiment setup (Courtesy of Christian Silva and Chul Min Yeum)

5.1.2 Results

Each vehicle crossing produces 12 acceleration responses. Using correlation, a perfect vehicle classification is achieved with a match of all 12 acceleration responses. Nine response matches, 75% of perfect classification, is used to classify a vehicle satisfactorily. Otherwise, it will be unclassified (UC). A total of 23 rounds are conducted. In each round, 22 crossings, which produce 264 acceleration responses, are used for training and the remaining crossing, 12 acceleration responses, for testing. The results are summarized in Figure 5.2 in chart and confusion matrix form.

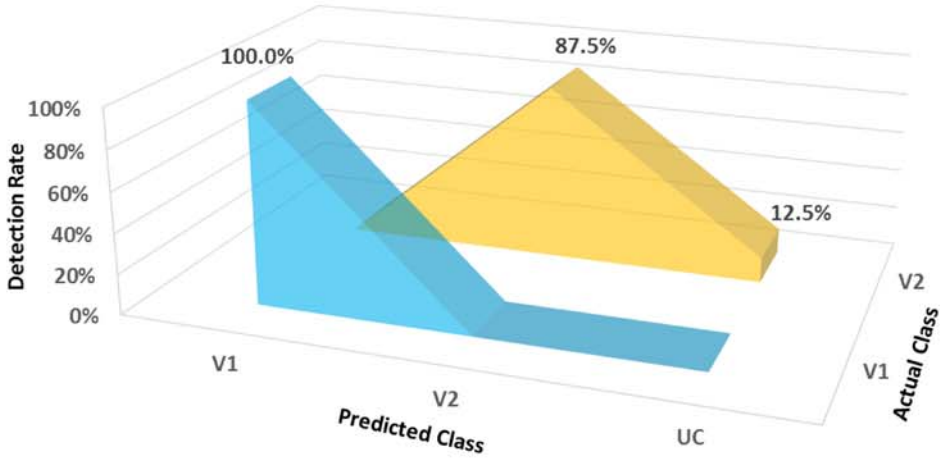

	V1	V2	UC
V1	100.0%	0.0%	0.0%
V2	0.0%	87.5%	12.5%

Fig. 5.2. REB experiment results

The results are very good, yielding an average of 95% detection rate. Vehicle crossings prove to create distinct responses, despite the similarity between vehicles, as shown in figure 5.3. The experiment demonstrates that for a specific set of parameters with relatively similar low weight vehicles crossing the bridge, the detection rate achieved is above 90% overall. In one round, Vehicle 2 is not classified properly, which may be attributed to the low weight per axle but due to limited data, results cannot be conclusive. The creation of distinct features in the spectrograms are directly

related to the axle distance, weight, and dynamics of the vehicle when coupled with the bridge.

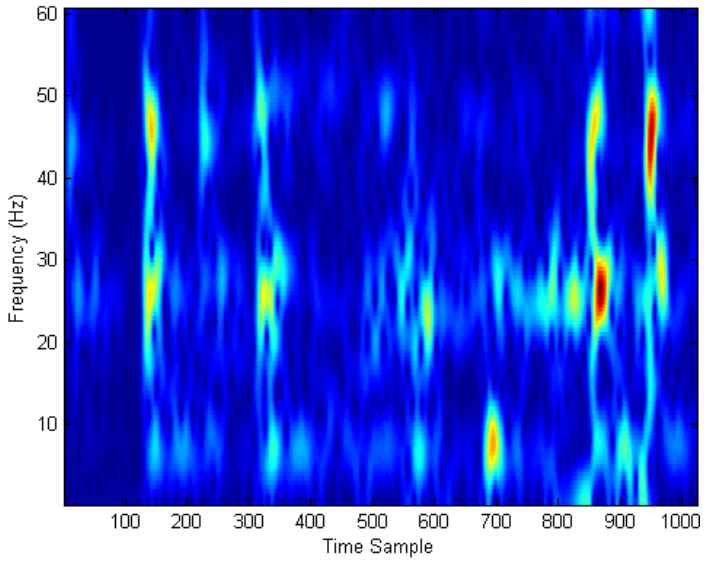

(a) Vehicle 1 response

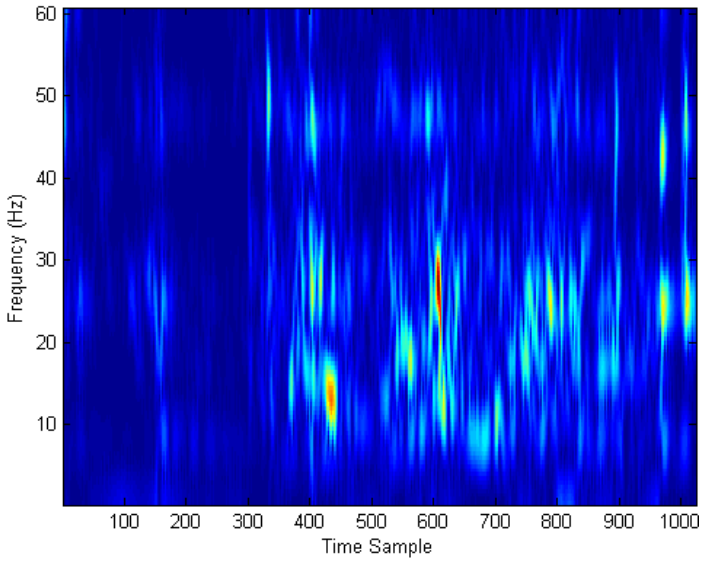

(b) Vehicle 2 response

Fig. 5.3. Acceleration responses for vehicles 1 and 2

Remarks: The experiment's success is directly related to the small number of vehicles and fixed setup condition. A sufficient amount of training and data points will yield good results. Although the results are promising and distinct responses are produced in the REB, further parameter variations must be studied when bridge access is available such as: additional vehicles, varying axle loads and distances, and setup variation. However, the intent of the experiment is met, showing that vehicle crossings produce distinct response spectrograms that can be detected and classified.

5.2 Laboratory Experiment

A scaled bridge is developed and exposed to different parameters and conditions with relative ease. The purposes of this experiment are to: demonstrate that distinct patterns are produced per vehicle despite setup, determine if small variation in speed affects the algorithm, and explore the sensitivity of the results to soil variation.

5.2.1 Setup

A small ditch, with enough clearance for deflection, is created to emplace the bridge and perform the testing. Table 5.2 shows the parameters used.

Table 5.2.
Laboratory scale bridge experiment parameters

Parameter	Explanation
Length	Approximately 4.4 meters
Vehicles	6 variations
Soil	Gravel (B1), rubber pads (B2), and wood (B3)

To obtain the vertical acceleration responses, eight accelerometers, four per side, are located along the length of the bridge. Figure 5.4 shows the bridge setup and accelerometer locations.

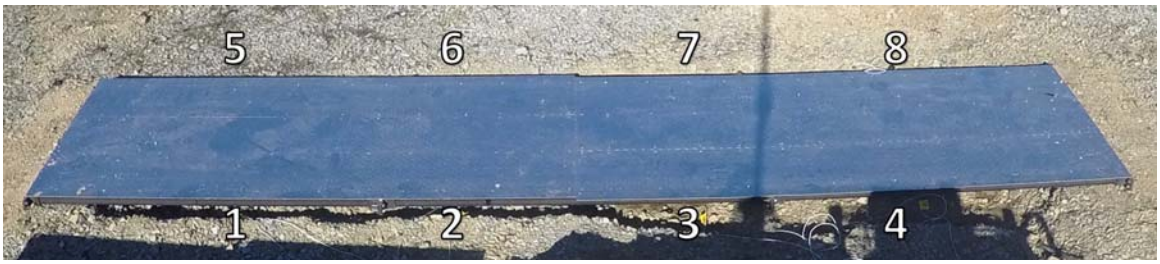

(a) Accelerometer locations

(b) Isometric view

Fig. 5.4. Scaled bridge with accelerometer locations

The bridge is easily moved manually to test the three different soil parameters mentioned in Table 5.2. Once emplaced, six vehicles cross the bridge 18 times, six times per setup condition, three times per direction. Figure 5.6 shows the vehicles utilized.

Vehicles 1, 2, 3, and 5 are four wheel, two axle, vehicles while Vehicles 4 and 6 are two wheel vehicles, one axle and two axle, respectively. The number of vehicles, along with wheel and axle variation, adds to the realism of field conditions. This

(a) Vehicle 1 (b) Vehicle 2 (c) Vehicle 3

(d) Vehicle 4 (e) Vehicle 5 (f) Vehicle 6

Fig. 5.5. Vehicles used in laboratory experiment (From [30])

variation imitates the challenges of obtaining enough distinct features to individually detect vehicles. Vehicle 1 and 2 are exactly the same and serve as a control vehicle.

To provide additional variation in test conditions, simulating realistic uncertainties, the vehicles are pulled by three different persons, taking three to six seconds to cross. The speed, although not constant, does not vary much thanks to the use of a ground guide. This mimics the actual scenario of small speed variation and driver variation. Speed would be easier to control on the REB by a combination of speedometer, ground guides, and speed signs.

With eight accelerometers installed, each vehicle crossing produces eight acceleration responses, 48 per soil parameter, 144 in total. Since there are six vehicles, six crossings, and three setups, data from 108 total crossings are collected and 864 re-

sponses are obtained. The acceleration data is captured manually and later cropped, as explained in section 3.2.1, to the specific time span when vehicles are crossing. Below are the specific tests that are examined:

Test A Determine soil parameter using reference vehicle

Test B Determine overall detection rate with all setups

Test C Determine detection rate with different training and testing setups

These tests are designed to determine the sensitivity of the results to soil variation, to assess overall algorithm performance under various training and testing conditions, and to consider the effects of vehicle response similarity and the impact of speed variation.

5.2.2 Acceleration Results

A total of 108 crossings, 864 acceleration results, are obtained. Visual inspection of the acceleration results obtained in the experiment, shown in Figure 5.6, demonstrate distinguishable patterns between vehicles. Vehicle 1 and 2 responses are almost the same, since they correspond to two vehicles with the same model number. These patterns will help in classifying the vehicle.

5.2.3 Test A Results

This test aims to determine if a reference vehicle can be used to determine the soil condition. Figure 5.7 shows the spectrograms of Vehicle 4 with different soil conditions. B1 refers to gravel, B2 refers to rubber pads, and B3 refers to wood.

The impact of soil variation can be seen visually, which indicates that it is likely that the algorithm will be able to detect the soil condition. All setups have features between 5 and 20 Hertz, but B2 and B3 show strong features at approximately 32 and 45 Hertz, respectively.

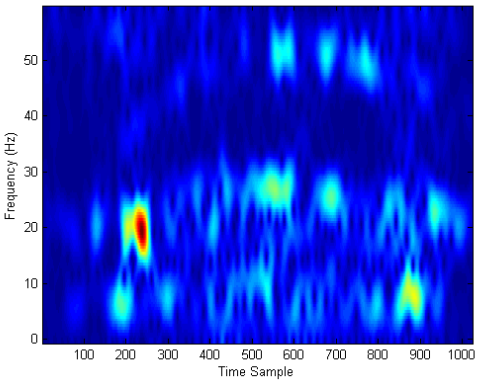

(a) Vehicle 1

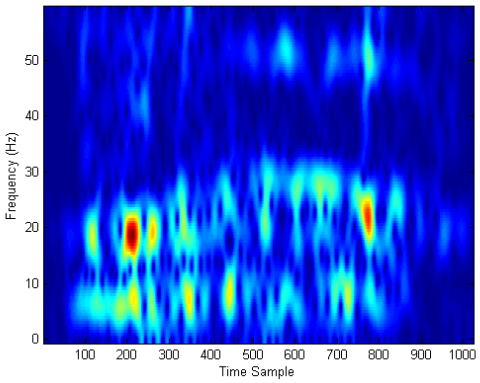

(b) Vehicle 2

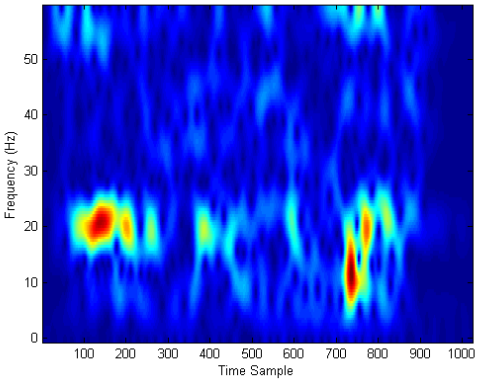

(c) Vehicle 3

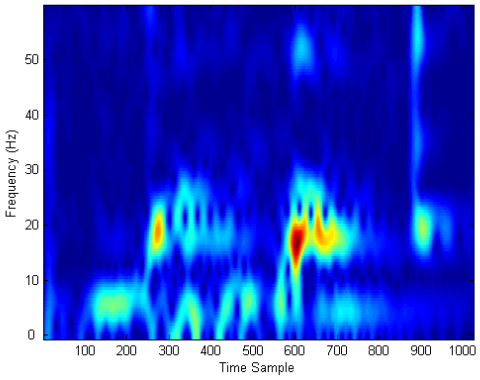

(d) Vehicle 4

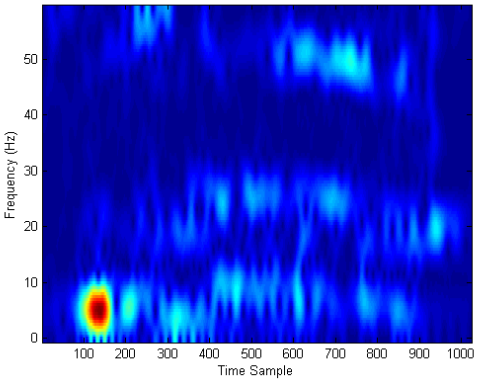

(e) Vehicle 5

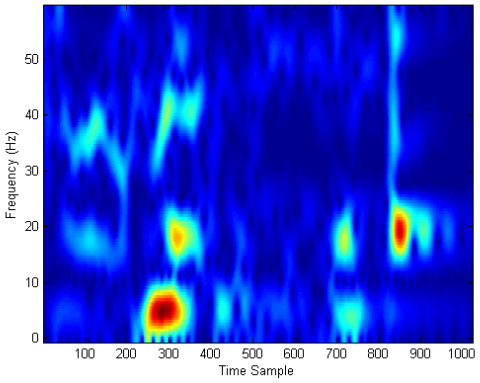

(f) Vehicle 6

Fig. 5.6. Vehicle spectrograms produced when bridge is placed on gravel

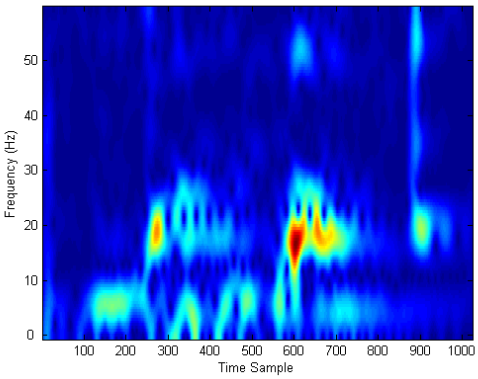

(a) B1 soil (Gravel)

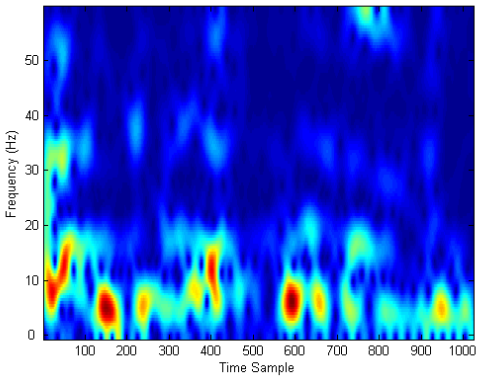

(b) B2 soil (Rubber mats)

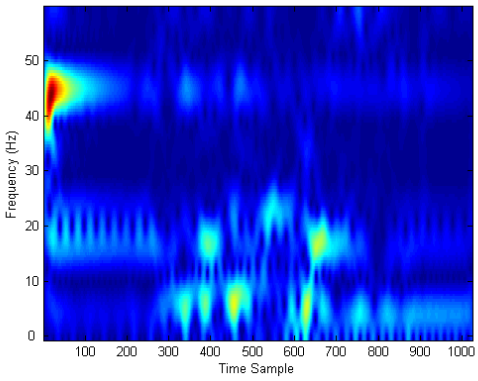

(c) B3 soil (Wood)

Fig. 5.7. Vehicle 4 responses for 3 soil conditions

Hence, Vehicle 4 is considered the reference vehicle and is thus the only one tested, representing the REB CBT. In the field it is likely that this vehicle would be used as a reference vehicle. Using only Vehicle 4 data, one crossing response is used for testing while the other 17 are used for training. There are a total of 18 rounds to account for all possible scenarios. This simulates the database of various bridge setups that would exist in an actual mobile bridge.

To discern which soil condition is selected, a binary decision is made between B1 and B2, B1 and B3, and B2 and B3. For the three binary decisions, the eight accelerations will be forced to be classified as either one of the two soil condition

options. Once all the possible binary decisions are classified as either B1, B2, or B3, the results for each soil condition is added. A perfect classification will yield a maximum of 16. Here, a total of 12, 75% of perfect classification, is used to classify a soil parameter satisfactorily. Otherwise, it is UC. Figure 5.8 shows the results for the 18 rounds of testing in both graphical and confusion matrix form.

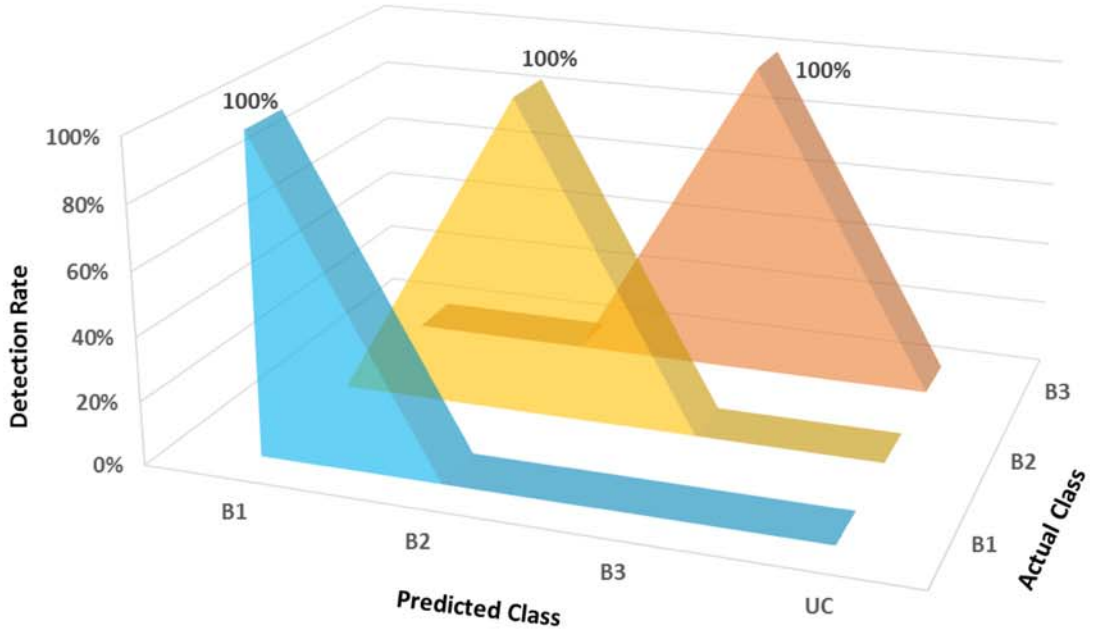

	B1	B2	B3	UC
B1	100%	0%	0%	0%
B2	0%	100%	0%	0%
B3	0%	0%	100%	0%

Fig. 5.8. Test A results

The classification of the reference vehicle works very well, yielding distinct features for each soil condition. The algorithm is able to extract enough features and accurately determine the right setup 100% of the time. It also shows the importance of acquiring training data from multiple setups to ensure a good match. Determining a bridge setup just after emplacement can reduce uncertainty. For example, the database created for this case has 108 crossing responses, 864 classifiers. If the soil

condition is determined each time the bridge is emplaced, the possible cases for subsequent vehicle crossings is reduced to 36 crossing responses, 288 acceleration responses. This improves the likelihood of detecting the right vehicle by removing irrelevant cases from consideration.

The resulting classifiers also show how alike each setup is to one another as follows: B1 to B3, B2 to B1, and B3 to B1. This alikeness is important to note because testing all possible soil conditions is too costly and time consuming. However, this results indicate a few discrete cases will suffice. In section 5.2.5 the similarities found are examined to determine how they affect the results.

Remarks: The use of a reference vehicle to reduce training required for the database, and increase the set of possible outcomes, helps focus the detection of vehicles. Reference vehicles can be used and implemented in the field, as they are readily available. They do not add additional time nor steps to the current procedure and provide insight into the behavior of the bridge. A reference vehicle, such as the CBT, will play a supportive role in the classification scheme and it is recommended that this approach be considered in the implementation.

5.2.4 Test B Results

This test studies the overall detection rate using all of the data obtained. Figure 5.9 shows different vehicle crossings with different soil conditions. Vehicles 1 through 6 are abbreviated as V1 through V6. Figure 5.9 sheds light into what the algorithm aims to accomplish as it classifies the vehicles. Visually, B1 and B2 produce similar response spectrograms while B3 produces different distinguishable patterns. As a reminder, Vehicle 1 and 2 are the same vehicle. Vehicles 1, 2, 3, and 5 maintain their general response characteristics across soil conditions without much variation. However, Vehicle 4 and Vehicle 6 responses vary greatly between setups. This differences across setups is not examined in this test, but it is studied in section 5.2.5.

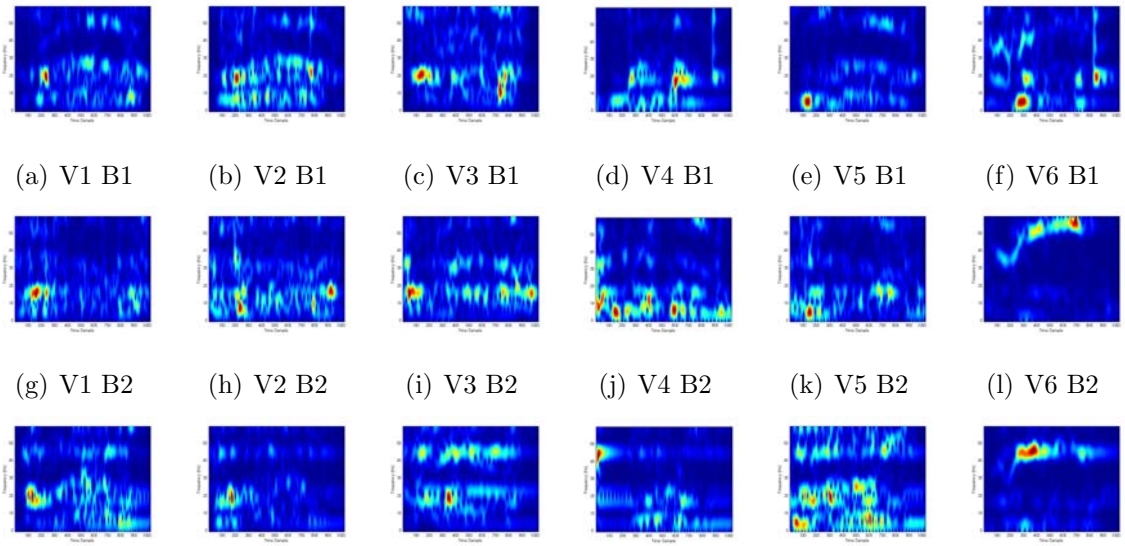

(a) V1 B1 (b) V2 B1 (c) V3 B1 (d) V4 B1 (e) V5 B1 (f) V6 B1

(g) V1 B2 (h) V2 B2 (i) V3 B2 (j) V4 B2 (k) V5 B2 (l) V6 B2

(m) V1 B3 (n) V2 B3 (o) V3 B3 (p) V4 B3 (q) V5 B3 (r) V6 B3

Fig. 5.9. Vehicle spectrograms under gravel setup

Here, the vehicle classification results are examined by taking one of the 18 crossings per vehicle for testing, while the remaining 17 crossings per vehicle are included in the larger training data sets. There are six vehicles, six runs, and three setups, for a total 108 rounds to account for all possible scenarios. Thus, each round uses 108 crossings, six for training and 102 for testing. As mentioned earlier, each crossing produces eight acceleration responses.

To classify properly, a binary code between Vehicles 1 through 6 is created with 10 possible combinations, similar to Test A but with vehicles instead of soil conditions. Some binary classifiers are Vehicles 1 and 3, 3 and 5, and 5 and 6. Vehicle 1 and 2 share the same binary classifiers because they are the same vehicle model. A perfect classification outcome would provide a maximum of 32. A total of 24, 75% of perfect classification, is defined as a satisfactory classification. If 24 is not reached, then the vehicle is considered UC. Figure 5.10 shows the results for all the rounds in graphical and confusion matrix form.

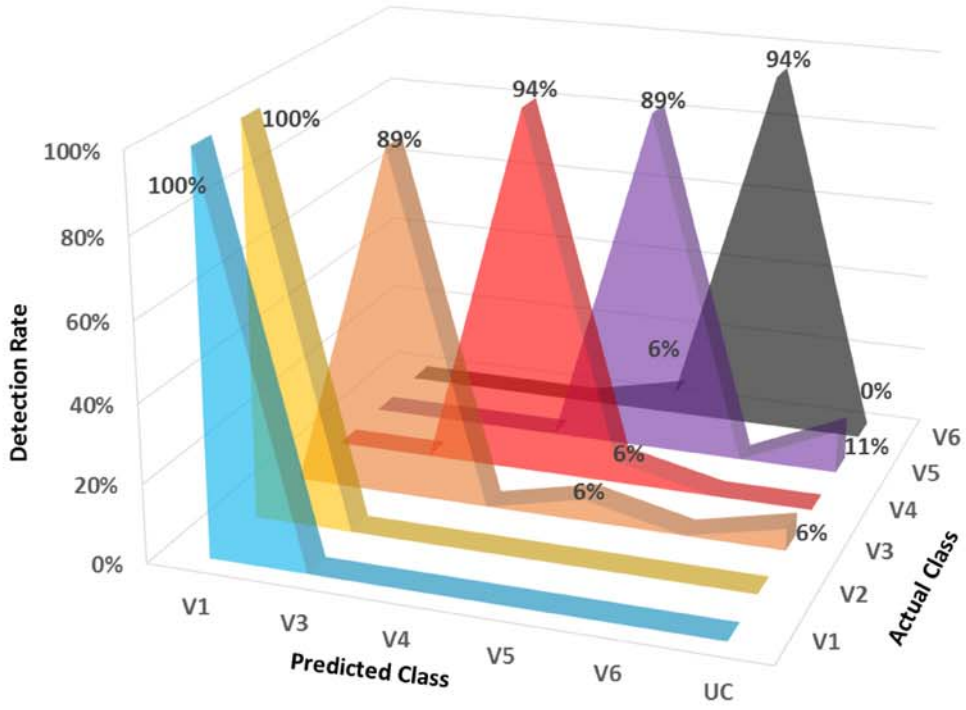

	V1	V3	V4	V5	V6	UC
V1	100%	0%	0%	0%	0%	0%
V2	100%	0%	0%	0%	0%	0%
V3	0%	89%	0%	6%	0%	6%
V4	0%	0%	94%	6%	0%	0%
V5	0%	0%	0%	89%	0%	11%
V6	0%	0%	0%	6%	94%	0%

Fig. 5.10. Test B results

The results average a 94% detection rate. Despite the minor mis-classifications in some rounds, the overall performance surpasses the stated goal. This demonstrates that even though several setup conditions exist in the database, distinct features are still matched to its closest vehicle. It also shows that, in some cases, distinct features are extracted and kept fairly similar among the three setups, as shown with Vehicles 1, 2, 3, and 5 in Figure 5.9.

This study highlights that when testing occurs with one of the three soil conditions included in the training set, the detection rate meets the requirement. It also helps strengthen the idea that in some vehicles, distinct patterns can be extracted amongst different setups and small speed variation does not impact the algorithm. Despite the good results, it is improbable that the field condition will exactly match the training soil parameters. The difference in field and training conditions will be studied in the following section.

5.2.5 Test C Results

This test is designed to explore the sensitivity of the results to soil variation when the testing and training classifiers are different at each round. Figure 5.9, in section 5.2.4, shows the impact of soil variation in the spectrograms created. Soil variation is a key aspect to study, as the emplacement occurs at various locations, each with boundary conditions and Soil Bearing Capacity (SBC). The manual states that bridge emplacement can occur if the SBC is higher than 450 kN/m^2 [7]. In field applications there is not enough time for soil tests and therefore, a visual inspection and subjective emplacement consolidation suffice to determine if a bridge is safe to cross. This specific sensitivity study provides an understanding of how the setup may affect the detection rate and how it can be controlled to improve results.

Here, training occurs in one soil condition and testing occurs in the other two soil conditions. In section 5.2.3, close relationships between soil conditions are found to be as follows: B1 to B3, B2 to B1, and B3 to B1. If the vehicle being tested has a soil condition of B1, B2, or B3, the training classifiers to be used are only from the soil condition B3, B1 or B1, respectively. For example, if the testing vehicle used crossed at a soil condition B1, the training classifiers used are those created from B3 crossings. This difference closely matches field scenarios and provides guidance on how to reduce the impact of soil conditions. Here, all setup condition are determined using reference Vehicle 4, studied in section 5.2.3.

Vehicle classification occurs by taking one of the six crossings data per vehicle per soil condition for testing, while the closest soil condition 6 crossings are used for training, as mentioned earlier. Thus, in the testing phase, the classifiers used are based entirely on crossings with different soil conditions data. There are six vehicles, six runs, and three setups, for a total 108 rounds to account for all scenarios. To classify the vehicles, a binary code between Vehicles 1 through 6 is created with 10 possible combinations, exactly similar to Test B. A perfect classification outcome would provide a maximum of 32. A total of 24, 75% of perfect classification, is defined as a satisfactory classification. If 24 is not reached, then the vehicle is considered UC. Figure 5.11 shows the results for all of the rounds in graphical and confusion matrix form.

The detection rate averages 76%, with individual accuracies exceeding 66% except for Vehicle 3, which obtained a 44%. These results do not satisfy stated requirements. When using different bridge setups for training and testing, the accuracy is reduced considerably. The difference in classifiers created present a challenge for classification that must be addressed. Since the results need improvement, additional soil condition cases need to be examined to determine how many to use in training for success. However, another option is to create a group index.

A group index should take into account the similarity of the responses as well as the number of full load cycles it induces on the mobile bridge. Heavier vehicles produce larger amplitude responses when crossing a bridge, inducing more full load cycles. As more full load cycles are induced, the more the finite life gets reduced. Thus, to develop a group index, thorough analysis of full load cycles should be performed in the future.

Remarks: There are more challenges in capturing individual vehicle classification if the training data set does not include the soil condition of the testing case. Satisfactory results are obtained when the training and testing soil conditions match, as shown in section 5.2.4. However, it is impossible to create classifiers for all possible scenarios. To provide good detection rates under field imple-

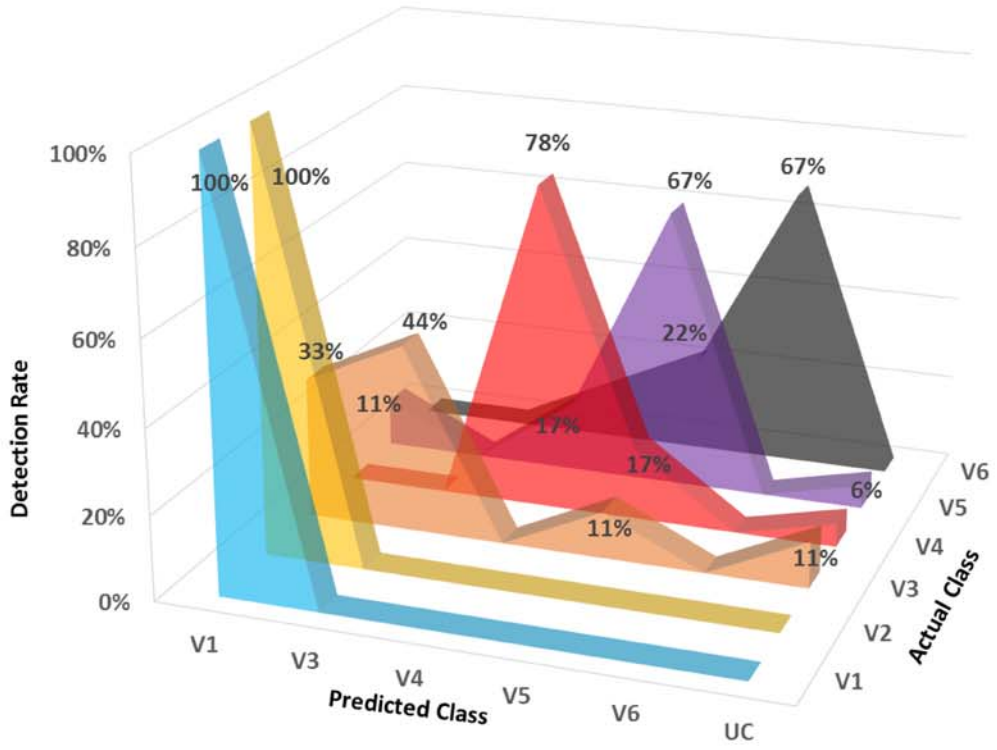

	V1	V3	V4	V5	V6	UC
V1	100%	0%	0%	0%	0%	0%
V2	100%	0%	0%	0%	0%	0%
V3	33%	44%	0%	11%	0%	11%
V4	0%	0%	78%	17%	0%	6%
V5	11%	0%	17%	67%	0%	6%
V6	0%	0%	11%	22%	67%	0%

Fig. 5.11. Test C Results

mentation, training should occur under various soil conditions. The number of cases for real world implementation should be determined for the REB.

5.3 Summary and Implementation Recommendation

These experiments demonstrate the algorithm's success under various conditions and parameters. The REB experiment shows that distinct acceleration features may

be extracted and matched to a specific vehicle with high success. These results are above 90%, despite both vehicles being relatively similar.

The laboratory experiment demonstrated many important aspects of the algorithm. Test A showed that a reference vehicle, Vehicle 4, can be used to distinguish setup conditions. Test B showed that with various vehicles and soil conditions, unique acceleration features are still produced, and when classifiers are trained and tested with given soil conditions, individual vehicles are detected with relative ease. Finally, Test C showed that if the training and testing soil conditions differ, which is similar to field applications, the individual vehicle classification is not satisfactory and the number of soil conditions to be included in the training data requires examinations.

These results are used to compile a recommendation, shown in Table 5.3. For the experiments discussed here, these recommendations produce the best environment for achieving required detection rates.

Table 5.3.
Best parameter settings

Parameter	**Recommendation**
Vehicle speed	Control speed rnage with a ground guide or signs
Soil	Design training for low, medium and high SBC training classifiers
Index	Consider an appropriate grouping strategy

Further REB studies with a broader vehicle range up to MLC 50 and soil conditions is recommended to determine individual classification rates.

6. IMPLEMENTATION RECOMMENDATION

Based on the results of the experiments and simulations in the prior chapters, a procedure must be established to yield the most successful vehicle classification. A successful implementation reduces under-classification, does not add any additional time to the current procedure, and provides reliable detection rates, ensuring the safety of the structure and users. The following sections explain how the current procedure works, how it can be improved, and how it can be generalized for application to any mobile or temporary bridge structure.

6.1 Current Procedure

The REB can be emplaced, crossed, and retrieved in the field in under 10 minutes. Initially, the bridge is inspected visually by a technician, checking that the RSLI are not broken. Once it passes inspection, it is transported to the deployment site. Once placed, the CBT crosses the bridge to ensure it is safe. After it is used, the CBT can retrieve the bridge and continue its mission. This process is summarized in Figure 6.1.

As demonstrated, the only indicator used now for bridge serviceability is the RSLI. If the RSLI break, the bridge is considered unserviceable and must be sent for repairs or retrofit. The user cannot predetermine when they will break due to the broad range of vehicles that cross. No accessible field data exists to show how many vehicle passes actually occur before failure. Therefore, the user and fabricator need to count vehicles passes to understand when and how the bridge fails. This is of great importance if the RSLI's break by accident, expending funds unnecessarily for both sides.

The bridge has proven to be successful in field operations. The quickness and effectiveness for crossing spans under 13 meters allows a wide spectrum of operations

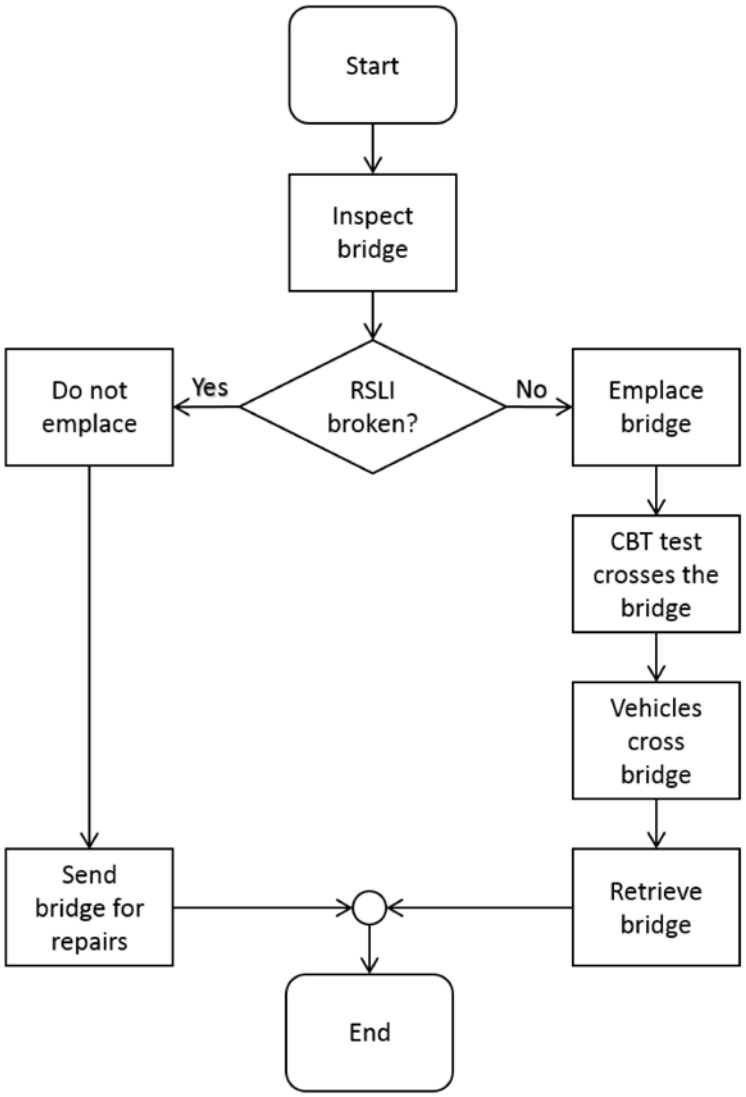

Fig. 6.1. Current REB procedure

worldwide, especially in disaster relief. To continue promoting the usefulness of the bridge, the new procedure, outlined in the following section, will not add additional field time to the emplacement process and ensure a high success ratio.

6.2 REB Procedure Recommendation

The recommendations here are intended for future REB applications. The goals of the procedure are: (1) ensure reliable detection rates are achieved and (2) add

no additional time to current process. It is impossible to predict and train for all possible parameter variations. As more REB's are used in the field, more information regarding their actual use will be available. Using the results from sections 4 and 5, a practical approach can be established to create an environment where vehicle detection is at its highest. A classifier database must be created with sufficient data and cases to address the most common vehicles and parameters to which the bridge is applied.

6.2.1 Training Classifier Database

The database will support training of the classifiers and thus its design should address a range of realistic variations in the following parameters: soil, bridge length, type and speed of vehicles, noise, and sensor filter. Tables 4.4 and 5.3 show the summarized recommendations per the numerical and experimental investigations that will be applied.

The REB is considered a quick emplacement bridge that does not need a thorough soil study. Therefore, it can be assumed that as long as the bridge does not sink or presents an unsafe behavior while being crossed, it will be used. The manual states that it can be emplaced on a variety of soils, like loose coarse sand to overlaying rock, which achieve an SBC above 450 kN/m^2 [7]. The results in 5.2.5 help in understanding that when the training and testing classifiers are not from the same soil parameter, individual classes are hard to detect. Therefore, group indices should be applied. Using this same guidance, producing training classifiers for three variations of soil with SBC's of approximately 500, 900, and 1300 kN/m^2 can help provide sufficient data for training.

It is impossible to ensure a specific bridge length is used for every field emplacement. Length is the most sensitive parameter and the more information available, the better the detection rate. The results in section 4.3.2 show that small ranges in bridge lengths provide the best environment for detection. Using this guidance, it

is recommended that the database be trained for 11 bridge length cases, at integer lengths from 3 to 13 meters. It should be discussed if short span bridge lengths, under 4 meters, should be considered, since they may not be used frequently in the field.

Vehicle speed cannot be controlled nor considered constant while crossing the bridge. However, sections 4 and 5 show that a small variations in speed, even while crossing, decreases misclassification. Such variations would likely be present, and should certainly be allowed in the training sets as well. The combined use of a ground guide, vehicle speedometer, and maximum and minimum speed signs can aid in enforcing limited variation of speed. With this is mind, it is recommended that the training classifiers be trained in three general speeds: 15, 25 and 35 km/hr. These three general speeds take into account the plus or minus $5km/hr$ variation, guaranteeing that each crossing is relatively close to a trained speed classifier.

The algorithm is effective under high noise ratios. Since environmental noise is hard to determine, training should be conducted using the most realistic field setting to decrease sensitivity. Section 4.3.4 showed that the algorithm readily tolerates up to an additional 10% noise for all bridge lengths, and up to 25% noise between 5 and 11 meters. Thanks to the high noise tolerance, multiple noise levels are not needed to train the classifiers.

Section 4.3.1 showed that the best low pass filter setting is half of the data rate and it is the recommended option here. Also, group indices provide the best vehicle classification results. It is recommended that training occurs with all vehicles that typically use the bridge and ensure all MLC classes are represented. This could yield a conservative number of 10 different vehicles. Once the training occurs, the similarities amongst vehicles should be studied to see what group index would be the best fit.

In summary, the following is recommended for creating the training database: 3 soils, 11 lengths, 3 speeds, 1 noise scenario, 1 filter setting, and 10 vehicles, for a total of 990 scenarios, 99 per vehicle. The database size can increase or decrease if parameters are added or subtracted, respectively. The accelerometer on the REB will be slightly off mid-span, which is better overall, as it can capture more bridge frequencies

than if it were located mid-span, as explained in section 6.3.2. To capture the change in vehicle direction, the training bridge could have an additional accelerometer installed to acquire the data on the other side of the bridge. This will only be used to capture training data and would double the amount of data acquired, improving the classifiers. Table 6.1 shows the summary of recommended parameters to create the database.

Table 6.1.
Training database parameters

Parameter	**Values**	**Variations**
Soil SBC	500, 900, and 1300 kN/m^2	3
Bridge length	3 to 13 meters, in integers	11
Vehicle Speed	15, 25, and 35 km/hr	3
Noise	Realistic field environment	1
Sensor filter	1/2 data rate	1
Vehicles	10 vehicles (MLC 4 to MLC 50)	10

The database can be created in two weeks or less, if all the vehicles are available and parameters are prepared. Once the database is created, only the classifiers will need to be saved in the memory of the accelerometer boards and maintained. A summarized flowchart of the database creation is shown in Figure 6.2.

6.2.2 Procedure Recommendation

The database creation allows the proposed recommendation to work as best as possible. Summarized in Figure 6.3, the proposal adds a second inspection layer, the engineer cell, and the CBT test crossing is now an algorithm calibration. The engineer cell is composed of engineers that design and maintain structures in a specific area of operation. These additional steps do not add any time to the current field application

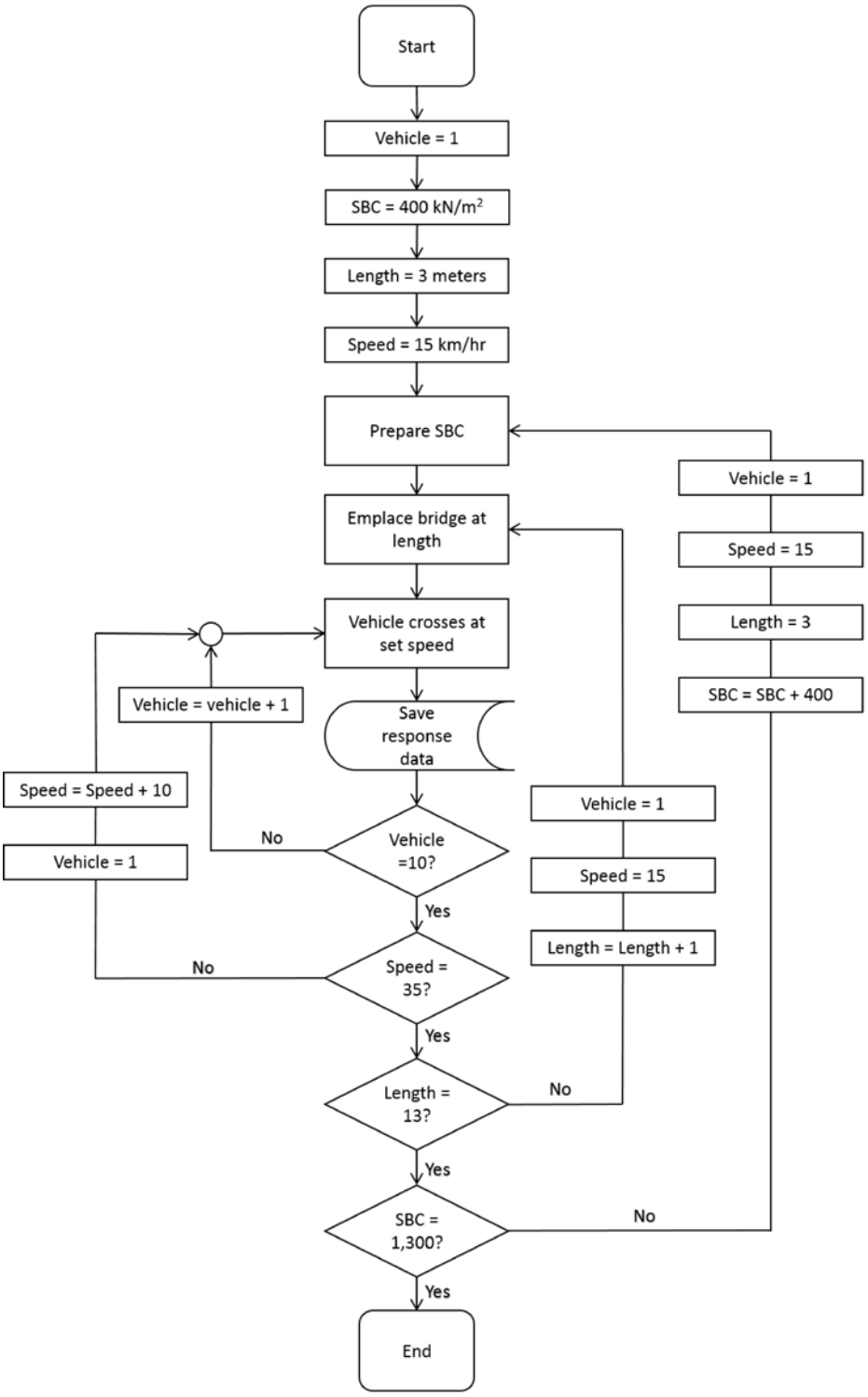

Fig. 6.2. Database creation

and it may save time and money when the engineer cell deems the bridge serviceable, despite broken RSLI.

The proposed process starts with visual inspection of the bridge RSLI, as it is a very important step that cannot be removed. If they are found to be broken, the engineer cell will be able to make a determination if the bridge is safe to use, based on the bridge vehicle histogram found in the memory. The fabricator and user currently use a procedure that allows them to calculate how many specific classes of vehicle can cross the bridge, known as finite life. The finite life calculation uses the stress ranges different classes produce and applies Miner's Law to determine the amount of passes left before a repair is needed. This procedure is described in AASHTO LRFD Bridge Design Specification [1].

Since the accelerometer on the bridge will track the vehicles histogram, finite life can be estimated at any point, despite broken RSLI. For example, if a bridge can handle 100,000 MLC 40 passes before failure and a local bridge database shows that 80,000 equivalent MLC 40 passes have occurred, then the bridge can still be used. This procedure saves time and money for both the user and fabricator, as the bridge is not sent for repairs before its useful life and missions are able to continue. Additionally, bridge repair timelines can now be estimated, better preparing both parties. It is important to note that if the engineering cell does not have enough data to make an informed decision, the RSLI will be the fall back safe plan to follow.

Once the bridge has been determined safe to use, the CBT can perform a test crossing. While crossing, the acceleration response is matched internally to the bridge database, calibrating it to a specific bridge length and soil range. As explained in sections 5.1 and 5.2, knowing specific parameters improves the detection rate drastically. This calibration reduces the number of classifiers from 990 to 120, improving the likelihood of correctly detecting the group. Once the soil and bridge length range are set, vehicles can cross. When a vehicle crosses, the speed is estimated and a speed range can be established. This improves the matching probability from 120 classifiers to just 80. Once the speed range is set, the response is compared against the

database and a match occurs. The match is then recorded in the lifetime histogram, the response is deleted, and new responses can be obtained. This internal process, explained in Figure 6.4, lasts less than a second, which provides enough time between vehicle crossings.

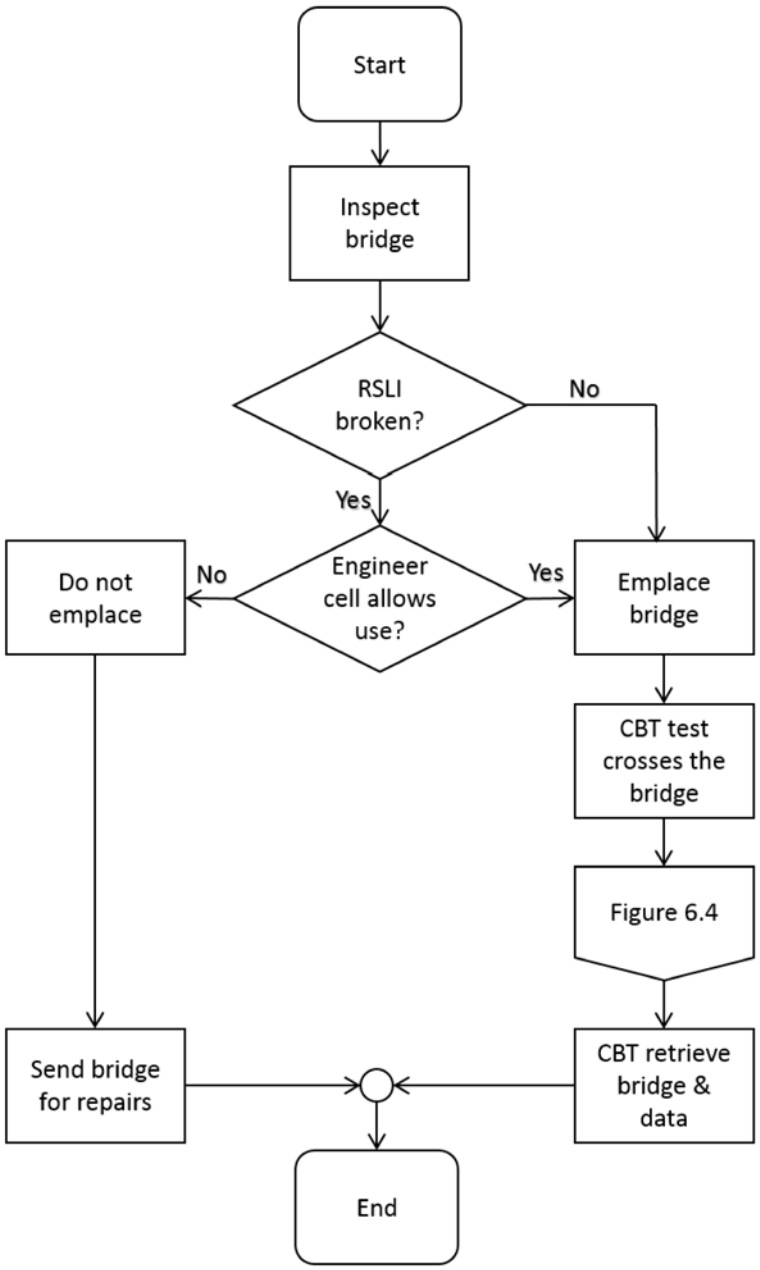

Fig. 6.3. Proposed procedure

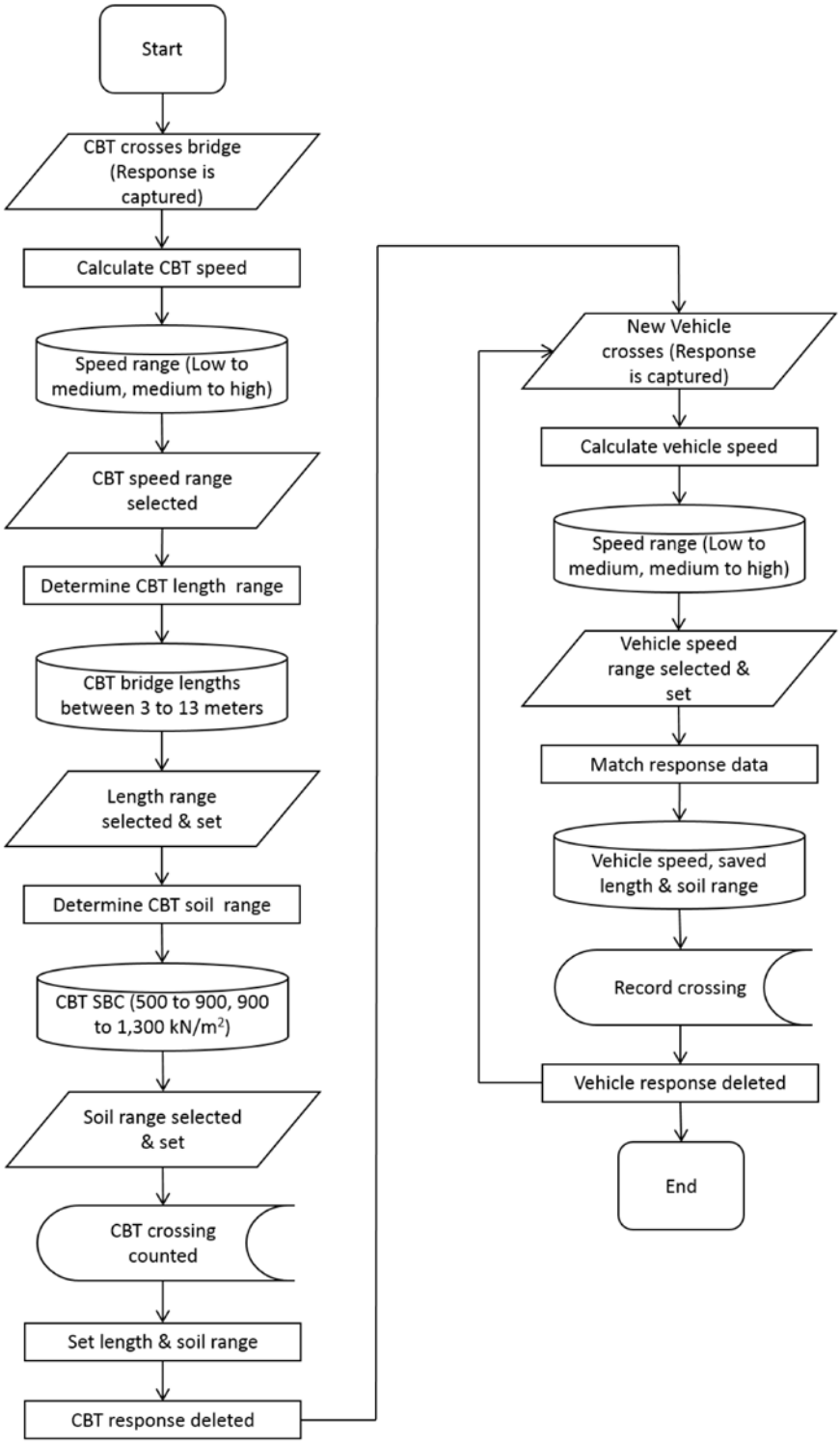

Fig. 6.4. Internal algorithm activities when bridge is emplaced

6.3 Generalized Bridge Application

The algorithm proved to be successful when applied to the REB and the laboratory scaled bridge. These results enhances its possibilities for general bridges. Mobile and temporary bridges, such as the armored vehicle launched bridge (AVLB) [40] and Acrow bridges [2], may benefit from this procedure. This section provides guidance on how to perform a generalized bridge application with the algorithm developed.

(a) Guanajibo, Puerto Rico (b) San Juan, Puerto Rico

Fig. 6.5. Temporary Acrow bridges

6.3.1 Assumptions

The basic premise that vehicles produce distinct features while crossing a bridge was proved, both numerically and experimentally. However, it was developed under a specific set of guidelines. Table 6.2 shows the guidelines to utilize the algorithm successfully. These assumptions present the best environment for application. If the bridge does not meet them, then a thorough study should be performed to determine viability.

Table 6.2.
General bridge application guidelines

#	Guidelines
1	Single span bridge
2	Only one vehicle crosses at a time
3	Low pass filter is used
4	Representative training data is available with varying parameters

6.3.2 Application

The REB procedure was developed based on a sensitivity study that considered various parameters. These parameters can change from bridge to bridge but a generalized method can be developed. The first step is to determine the type of accelerometer that will be used and its power demand. The accelerometer selection is very important, as it guides the cut-off frequency for the spectrograms as well as the power supply required.

After accelerometer selection, the parameters of the bridge should be studied to determine which are required for training. If the bridge will be as mobile as the REB, then multiple training scenarios have to be conducted. However, if a temporary bridge will be placed in a specific area for a longer time, the training could be conducted within those guidelines. This means that only one soil and length parameters are needed. These parameters are used to study the bridge frequencies.

Bridge frequencies are needed to determine the best placement for the accelerometers. It is recommended that the accelerometers be placed in a location where it can maximize the reading of multiple frequencies. For example, if located mid-span, the user may lose readings from the second and fourth mode frequencies. However, if they are located off center, it will capture them. Figure 6.6 shows poor accelerometer locations that should be avoided while looking at the first four modes.

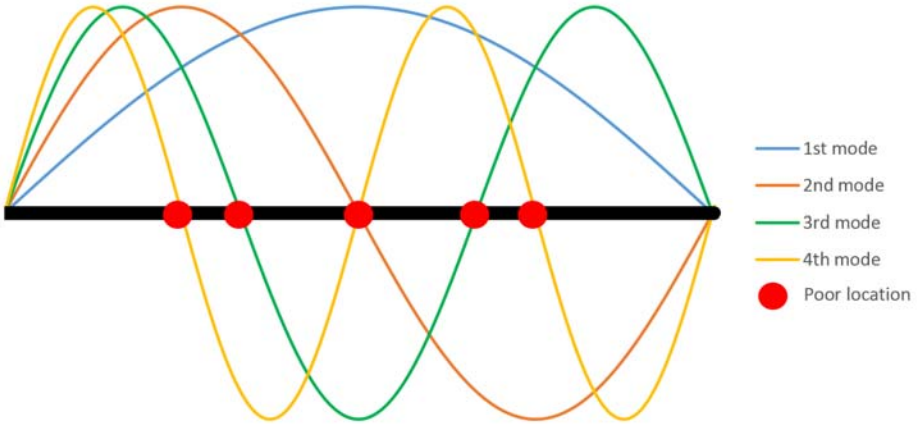

Fig. 6.6. Poor accelerometer locations

The accelerometer placement is also related to the number of accelerometers that will be used. If only one accelerometer is used, then only one classifier is trained per crossing and the closest response match will determine the classification. However, if multiple accelerometers are used, a binary classifier could be developed to create a true group index match of 75%, similar to section 5. The user should determine if they should use one or more accelerometers.

Once all the parameters and accelerometer placement have been decided, a database can be created. Figure 6.2 shows the database flowchart for the REB that can be modified to meet any bridge needs. The database should include the most representative vehicles and conditions. But once trained, the bridge is ready for use.

Remarks: Temporary and mobile bridges are used in military and emergency situations, providing access and mobility to accomplish a mission. These varying applications need active monitoring to ensure it is safe to use. The procedures outlined, based on the recommendations of section 6.2.2, provide the means to implement the algorithm to temporary bridges. The implementation can help monitor bridge activity, determine serviceability and save money.

7. SUMMARY AND CONCLUSIONS

A vehicle classification algorithm was successfully developed to determine the class of vehicle crossing a mobile bridge using acceleration responses. It shows promising results in applications for single span mobile bridges such as the REB. The following conclusions and future work recommendations lay the groundwork for real world applications.

7.1 Important Conclusions

The results of numerical and experimental studies demonstrated that when a vehicle crosses a mobile bridge, it produces distinguishable features that can be used to create a strong classifier. The strong classifier is saved in a training database and applied to future crossings to determine the vehicle class. This classification is used to create a vehicle histogram that will aid in determining bridge serviceability. To determine the best environment for vehicle detection, numerical and experimental investigations were conducted.

The experiments determined the sensitivity of the results to the following parameters: bridge length, vehicle speed, soil condition, environmental noise, and accelerometer filter. These studies guided an experimental and practical implementation recommendation.

The numerical study provided insight into the following parameters: accelerometer filter, bridge length, vehicle speed, and noise. The accelerometer filter study showed that some filtering is better than none. When anti-aliasing filtering was applied, half data rate filtering performed overall better than quarter data rate filtering. Thus, half data rate filtering is the recommended procedure.

The second parameter studied was bridge length. The bridge length results demonstrated the most sensitivity, due to the change in the natural frequencies of a bridge when the length changes. The spectrograms created are limited herein to a cut-off frequency of 60 Hertz, which decreases the amount of distinguishable features detected in very short span bridge lengths of three meters and below. The shorter the bridge, the higher the natural frequencies when bridge properties remain constant. However, if a training database is created with sufficient representative bridge lengths, the results are able to meet the stated requirements satisfactorily. Therefore, creating a database with sufficient representative bridge lengths will yield positive results.

The third parameter studied was vehicle speed. Vehicle speed is difficult to control in the real world, as it depends on the driver and mission. It was determined that the algorithm performs well under a speed range variation of plus or minus $5km/hr$. Additionally, if ground guides or speed signs are used, the speed is easier to control. Thus, based on the results herein, a training database with at least three speeds should be created. Additionally, vehicle speed should be controlled while crossing a bridge to decrease the sensitivity of the results.

The fourth parameter studied was noise. The REB can be placed in a wide array of environments with different noise levels. It was determined that noise does not impact the performance of the algorithm much, as long as the training occurs in a reasonably realistic noise environment. Additionally, noise tolerance can be as high as 25% for some cases. Therefore, the REB should be emplaced in the most realistic field environment to train the classifiers for the algorithm.

A second investigation was conducted experimentally. To physically validate the algorithm, experiments are conducted on the REB and a laboratory scaled bridge. The REB experiment demonstrated that, under a specific set of parameters, vehicles produce distinct features and small speed variation does not impact the method. To further study real world impacts, a laboratory scaled bridge was studied. The scaled bridge provided insight into the fifth parameter, soil condition. Numerous vehicles and drivers cross the bridge, simulating realistic uncertainties. It was demonstrated, yet

again, that vehicles produce distinguishable features while crossing a mobile bridge, even with small speed variation. Additionally, some vehicles maintain similar general spectrogram features under different soil conditions. Also, reliable results are obtained when training and testing occurs in the same soil condition. However, Test C demonstrated that when training and testing soil conditions differ, vehicle classification is reduced.

These results were used to develop a practical implementation procedure for the REB. A database with multiple parameters was recommended for further implementation studies. These recommendations aim to provide the best environment to produce reliable results.

7.2 Future Work

The numerical and experiment studies are quite successful and suggest a procedure to follow for future studies. It is recommended to perform additional experiments before real world application. The following recommendations are made to guide further studies.

1. A full REB experiment should be conducted to collect sufficient data sets to evaluate the sensitivity of the results to varying parameters. The parameter variation could be studied as recommended in section 6 or as appropriate.

2. The full load cycles induced by different vehicles needs to be considered. The results, along with the spectrograms created, can help develop a group index.

3. All experiments should be conducted in an outside field setting, which is more likely to provide realistic ambient noise. This will demonstrate if the method works under a variety of expected conditions. Experiments inside a facility should be avoided.

4. Individual and correlation classification methods have different advantages and disadvantages. If additional accelerometers can be used in implementation, the correlation classification system can be studied.

5. Shorter spans and higher SBC's can increase the natural frequencies of a bridge. Examining the classification outcomes using higher cut-off sampling frequencies can help determine if the sampling frequency should be increased. This may also be done using wired accelerometers and processing the data to simulate a variety of choices.

6. The REB has a finite bridge life and its dynamic characteristics may change over time. Examine if and how bridge dynamics change over time and how robust the algorithm would be to such changes. This may also consider any differences in the dynamics of individual REB units.

7. When a vehicle enters the REB, it may be traveling at a high speed and may move the bridge horizontally. Over time, an unbalanced span bridge condition may occur, where one side has more support than the other. This unbalanced condition, along with induced horizontal accelerations, should be examined.

8. The REB is able to be emplaced at different shore heights. This change in elevation and this scenario should also be considered.

9. Future experimentation should be performed with the accelerometer that will be used in the method. This will provide the actual results expected to study before implementation.

10. Additional numerical studies should consider the dynamic interaction between the bridge and vehicles to closely match real world scenarios.

REFERENCES

REFERENCES

[1] AASHTO, *AASHTO LRFD Bridge Design Specifications*. American Association of State Highway and Transportation Officials, Washington, DC.

[2] Acrow. Acrow bridges. [Online]. Available: http://acrow.com/

[3] FHWA. National bridge inventory. [Online]. Available: https://www.fhwa.dot.gov/bridge/nbi.cfm

[4] L. M. Hively, R. K. Abercrombie, M. B. Scudiere, and F. T. Sheldon, "Error reduction for weigh-in-motion," 2008.

[5] L. D. Han, S.-S. Ko, Z. Gu, and M. K. Jeong, "Adaptive weigh-in-motion algorithms for truck weight enforcement," *Transportation Research Part C: Emerging Technologies*, vol. 24, pp. 256–269, 2012.

[6] R. J. Connor, "Behavior of metal structures," University Lecture, 2015.

[7] D. of the Army, *Operator's Manual for Rapidly Emplaced Bridge*, no. TM 5-5420-280-10.

[8] E. McEwen and G. Tsiatas, "Use of fatigue fuses for prediction of fatigue life of steel bridges," *Transportation Research Record: Journal of the Transportation Research Board*, no. 1544, pp. 71–78, 1996.

[9] Y.-J. Cha, J. Zhang, A. K. Agrawal, B. Dong, A. Friedman, S. J. Dyke, and J. Ricles, "Comparative studies of semiactive control strategies for mr dampers: Pure simulation and real-time hybrid tests," *Journal of Structural Engineering*, vol. 139, no. 7, pp. 1237–1248, 2013.

[10] X. Gao, N. Castaneda, and S. J. Dyke, "Real time hybrid simulation: From dynamic system, motion control to experimental error," *Earthquake Engineering & Structural Dynamics*, vol. 42, no. 6, pp. 815–832, 2013.

[11] B. Espion and P. Halleux, *Long-term Measurements of Strains with Strain Gauges and Stability of Strain Gauge Transducers*. HBM, 2000.

[12] P. Viola and M. Jones, "Rapid object detection using a boosted cascade of simple features," in *Computer Vision and Pattern Recognition, 2001. CVPR 2001. Proceedings of the 2001 IEEE Computer Society Conference on*, vol. 1. IEEE, 2001, pp. I–511.

[13] P. Viola and M. J. Jones, "Robust real-time face detection," *International Journal of Computer Vision*, vol. 57, no. 2, pp. 137–154, 2004.

[14] L. E. Y. Mimbela and L. A. Klein, "Summary of vehicle detection and surveillance technologies used in intelligent transportation systems," 2000.

[15] A. S. Nowak, H. Nassif, and L. DeFrain, "Effect of truck loads on bridges," *Journal of Transportation Engineering*, vol. 119, no. 6, pp. 853–867, 1993.

[16] L. A. Klein, *Sensor Technologies and Data Requirements for ITS*, 2001.

[17] B. McCall and W. C. Vodrazka Jr, "States successful practices weigh-in-motion handbook," 1997.

[18] Cardinal. Weigh-in-motion vehicle scales. [Online]. Available: http://wimscales.com/

[19] Cestel. Bridge weigh-in-motion. [Online]. Available: http://www.cestel.eu/

[20] A. K. Chopra, *Dynamics of Structures*. Prentice Hall, 2012.

[21] R. R. Craig and A. J. Kurdila, *Fundamentals of Structural Dynamics*. John Wiley & Sons, 2006.

[22] C. E. Silva, "Development, numerical demonstration and experimental verification of a method for model updating of boundary conditions," Ph.D. dissertation, PURDUE UNIVERSITY, 2014.

[23] R. Klette, *Concise Computer vision*. Springer, 2014.

[24] D. A. Forsyth and J. Ponce, "A modern approach," *Computer Vision: A Modern Approach*, 2003.

[25] W. T. Freeman and E. H. Adelson, "The design and use of steerable filters," *IEEE Transactions on Pattern Analysis & Machine Intelligence*, no. 9, pp. 891–906, 1991.

[26] Y. Freund and R. E. Schapire, "A desicion-theoretic generalization of on-line learning and an application to boosting," in *Computational Learning Theory*. Springer, 1995, pp. 23–37.

[27] C. M. Yeum and S. J. Dyke, "Vision-based automated crack detection for bridge inspection," *Computer-Aided Civil and Infrastructure Engineering*, 2015.

[28] MATLAB, *2013a*. Natick, Massachusetts: The MathWorks Inc., 2013.

[29] S. J. Dyke, "Structural dynamics," University Lecture, 2014.

[30] C. M. Yeum, S. J. Dyke, C. Silva, R. E. Basora Rovira, and J. Demo, "Rapid automated vehicle classification on mobile bridges using computer vision techniques," *Submitted to Computer-Aided Civil and Infrastructure Engineering*, 2015.

[31] R. S. Jakka and S. Garg, "Suitable triggering algorithms for detecting strong ground motions using mems accelerometers," *Earthquake Engineering and Engineering Vibration*, vol. 14, no. 1, pp. 27–35, 2015.

[32] R. G. Golla, "Real-time face detection and tracking," University Lecture, 2012.

[33] J. Friedman, T. Hastie, R. Tibshirani *et al.*, "Additive logistic regression: A statistical view of boosting (with discussion and a rejoinder by the authors)," *The Annals of Statistics*, vol. 28, no. 2, pp. 337–407, 2000.

[34] A. Torralba, "How many pixels make an image?" *Visual Neuroscience*, vol. 26, no. 01, pp. 123–131, 2009.

[35] S. V. Stehman, "Selecting and interpreting measures of thematic classification accuracy," *Remote Sensing of Environment*, vol. 62, no. 1, pp. 77–89, 1997.

[36] C. N. Van Groningen and R. A. Paddock, "Smart bridge: A tool for estimating the military load classification of bridges," Argonne National Lab., IL (United States), Tech. Rep., 1997.

[37] D. of the Army, *Engineer Reconnaissance (FM 3-34. 170 / 5-170 / MCWP 3-17. 4)*. Department of the Army, 2012.

[38] P. Piezotronics. Pcb model 333b40. [Online]. Available: http://www.pcb.com/Products.aspx?m=333B40

[39] m+p International. Data acquisition system. [Online]. Available: http://www.mpihome.com/en/

[40] FAS. M60a1 armored vehicle launched bridge (m60a1 avlb). [Online]. Available: http://fas.org/man/dod-101/sys/land/m60a1-avlb.htm

VITA

VITA

RICARDO EMILIO BASORA ROVIRA

CAREER OBJECTIVE

To obtain a Master of Civil Engineering with a focus on Structural Engineering.

EDUCATION

Master of Science in Civil Engineering	December 2015 Candidate
Purdue University - West Lafayette, IN	3.57 GPA
Master of Business Administration	2014
Webster University - St Louis, MO	3.88 GPA
Bachelors of Science in Civil Engineering	2010
University of Puerto Rico - Mayagüez, PR	3.39 GPA, Cum Laude (Honor)

WORK EXPERIENCE

Project Programmer, US Air Force

Hill AFB, UT November 2013 - July 2014

• F-35 construction program manager, coordinating 4 year construction plan

J7 Civil Engineering Director, US Air Force

Shindand AB, Afghanistan, Nov 2012-Nov 2013

• Lead engineer, project manager, design-build, advisor, and airfield engineer

Project Manager and Expeditionary Engineering Officer, US Air Force

Hill AFB, UT, April 2011 to November 2012

• Project designer, project manager, and unit deployment manager

ORGANIZATIONS

• American Society of Civil Engineers (ASCE)

• Intelligent Infrastructures Systems Laboratory (IISL)

• Society of American Military Engineers (SAME)